ACSL3 is a novel GABARAPL2 interactor that links ufmylation and lipid droplet biogenesis

ACSL3 is a novel GABARAPL2 interactor that links ufmylation and lipid droplet biogenesis

Franziska Eck[1], Santosh Phuyal[3], Matthew D. Smith[4], Manuel Kaulich[2], Simon Wilkinson[4], Hesso Farhan[3], and Christian Behrends[1]

[1]Munich Cluster for Systems Neurology (SyNergy), Medical Faculty, Ludwig-Maximilians-University München, Feodor-Lynen Strasse 17, 81377 Munich, Germany

[2]Institute of Biochemistry II, Goethe University School of Medicine, Theodor-Stern-Kai 7, 60590 Frankfurt am Main, Germany

[3]Institute of Basic Medical Sciences, Department of Molecular Medicine, University of Oslo, Sognsvannsveien 9, 0372 Oslo, Norway

[4]Cancer Research UK Edinburgh Centre, MRC Institute of Genetics and Molecular Medicine, University of Edinburgh, U.K., EH4 2XR

Correspondence to: christian.behrends@mail03.med.uni-muenchen.de

Keywords: GABARAPL2, ACSL3, lipid droplets, UBA5, ufmylation, ER-phagy

JCS Advance Online Article. Posted on 25 August 2020

Abstract

While studies of ATG genes in knockout models led to an explosion of knowledge about the functions of autophagy components, the exact roles of LC3 and GABARAP proteins are still poorly understood. A major drawback for their understanding is that the available interactome data was largely acquired using overexpression systems. To overcome these limitations, we employed CRISPR/Cas9-based genome-editing to generate a panel of cells in which human ATG8 genes were tagged at their natural chromosomal locations with an N-terminal affinity epitope. This cellular resource was exemplarily employed to map endogenous GABARAPL2 protein complexes using interaction proteomics. This approach identified the ER-associated protein and lipid droplet (LD) biogenesis factor ACSL3 as a stabilizing GABARAPL2-binding partner. GABARAPL2 bound ACSL3 in a manner dependent on its LC3-interacting regions whose binding site in GABARAPL2 was required to recruit the latter to the ER. Through this interaction, the UFM1-activating enzyme UBA5 became anchored at the ER. Further, ACSL3 depletion and LD induction affected the abundance of several ufmylation components and ER-phagy. Together, we describe ACSL3 as novel regulator of the enigmatic UFM1 conjugation pathway.

Introduction

From yeast to humans ATG8s are highly conserved proteins. While there is only a single Atg8 in yeast, the human ATG8 (hATG8) family is subdivided into the orthologs microtuble-associated protein 1A/1B light chain 3 (MAP1LC3) including LC3A, LC3B, and LC3C as well as γ-aminobutyric acid receptor-associated protein (GABARAP) including GABARAP, GABARAPL1 and GABARAPL2 (Slobodkin and Elazar, 2013). All six hATG8 proteins share the same, ubiquitin-like fold although they do not exhibit any sequence homologies with ubiquitin. However, within and between the ATG8 subfamilies, the amino acid sequences show high similarities (Shpilka et al., 2011). A major feature of LC3 and GABARAP proteins is their covalent conjugation to the phospholipid phosphatidylethanolamine (PE). This process is initiated by the cysteine proteases ATG4A-D that cleave all hATG8 family members to expose a C-terminal glycine residue and is followed by the activation of LC3s and GABARAPs through the E1-like activating enzyme ATG7. PE-conjugation of hATG8 proteins is subsequently accomplished in a concerted action of the E2-like conjugating enzyme ATG3 and the E3-like ligase scaffold complex ATG12-ATG5-ATG16L1. PE-hATG8 conjugates are reversible through cleavage by ATG4A-D (Mizushima et al., 2011).

The best understood function of hATG8s is in macroautophagy (hereafter referred to as autophagy) which is a highly conserved degradation pathway that eliminates defective und unneeded cytosolic material and is rapidly upregulated by environmental stresses such as nutrient deprivation. In the past years, it was shown that autophagy is capable of selectively recognizing and engulfing divers cargo such as aggregated proteins (aggrephagy), pathogens (xenophagy) or mitochondria (mitophagy) with the help of specific receptor proteins (Kirkin and Rogov, 2019). Initiation of autophagy leads to the formation of phagophores (also called isolation membranes) from preexisting membrane compartments, such as the ER. Elongation and closure of isolation membranes leads to engulfment of cargo inside double membrane vesicles termed autophagosomes. Fusion of autophagosomes with lysosomes forms autolysosomes in which captured cargo is degraded in bulk by lysosomal hydrolases (Dikic and Elazar, 2018). During this process, GABARAPs and LC3s are associated with the outer and inner membrane of phagophores and regulate membrane expansion (Xie et al., 2008), cargo receptor recruitment (Stolz et al., 2014), closure of phagophores (Weidberg et al., 2011) and the fusion of autophagosomes with lysosomes (Nguyen et al., 2016).

Besides autophagy, GABARAPs and LC3s are implicated in a number of other cellular pathways. For example, GABARAP was found as interactor of the GABA receptor and involved in its intracellular transport to the plasma membrane (Leil et al., 2004, Wang et al.,

1999), while GABARAPL2 was identified as modulator of Golgi reassembly and intra-Golgi trafficking (Legesse-Miller et al., 1998, Muller et al., 2002). GABARAPs were also found as essential scaffolds for the ubiquitin ligase $CUL3^{KBTBD6/KBTBD7}$ (Genau et al., 2015). Among others, LC3s have regulatory functions in RhoA dependent actin cytoskeleton reorganization (Baisamy et al., 2009) as well as in the regulation of ER exit sites (ERES) and COPII-dependent ER-to-Golgi transport (Stadel et al., 2015). This high functional diversity of GABARAPs and LC3s implies that these proteins are more than autophagy pathway components and that there are possible other unique functions of individual hATG8 proteins to be unraveled.

So far, interactome and functional analyses of LC3s and GABARAPs were mostly done in cells overexpressing one of the six hATG8 family members (Behrends et al., 2010, Popovic et al., 2012). This raises the concern that an overexpressed hATG8 protein might take over functions or interactions of one of the other family members due to their high sequential and structural similarity. A lack of isoform specific antibodies further complicates the analysis of distinct functions of hATG8s. To facilitate the study of endogenous GABARAPs and LC3s, it is important to generate alternative resources and tools such as the multiple hATG8 knockout cell lines (Nguyen et al., 2016) or the hATG8 family member-specific peptide sensors (Stolz et al., 2017). To circumvent the hATG8 antibody problem, we used CRISPR/Cas9 technology to seamlessly tag hATG8 genes at their natural chromosomal locations. The generated cell lines ($hATG8^{endoHA}$) express N-terminally hemagglutinin (HA)-tagged hATG8 family members at endogenous levels and are a powerful tool to study the functions of individual GABARAPs and LC3s. All created cell lines were tested for their correct sequence and functionality. As a proof of concept, we performed interaction proteomics with the $GABARAPL2^{endoHA}$ cell line and characterized the interaction with the novel binding partner ACSL3.

Results

Establishment of cells carrying endogenously HA tagged LC3s and GABARAPs

Complementary to our previously reported $LC3C^{endoHA}$ HeLa cell line (Le Guerroue et al., 2017) we sought to employ CRISPR-mediated gene-editing to generate a panel of cells in which the remaining five hATG8 family members are seamlessly epitope tagged at their natural chromosomal locations. To this end, we directed Cas9 to cleave DNA at the vicinity of the start codon of LC3 and GABARAP genes in order to stimulate microhomology-mediated integration of a sequence encoding for a single HA-tag using a double-stranded DNA donor molecule containing short homology arms (Kaulich and Dowdy, 2015). Briefly, we designed PCR

homology templates in which the blasticidine resistant gene, a P2A sequence and the open reading frame of the HA-tag were flanked by homology arms to the 5'UTRs and first exons of the LC3/GABARAP genes (Fig. S1A). In parallel, we designed single guide RNAs (sgRNAs) for all hATG8 genes except LC3C and cloned them into pX330, a SpCas9 expressing vector (Fig. S1A). We then transfected HeLa cells with corresponding pairs of homology template and sgRNA for each LC3/GABARAP gene. After selection with blasticidine, single cell clones were SANGER sequenced to confirm seamless and locus-specific genomic insertion of the HA-tag. While we obtained correct clones for GABARAP, GABARAPL1, GABARAPL2 and LC3B (Fig. S1B), cells that received the homology template and sgRNA for LC3A did not survive the antibiotic selection. We assume that this is due to the lack of LC3A in HeLa cells as it is reported that LC3A expression is suppressed in many tumor cell lines (Bai et al., 2012). Immunoblot analysis of the sequence-validated clones and the parental cells revealed the presence of the HA-tag in the engineered cell lines that corresponded to the size of the tagged LC3/GABARAP protein (Fig. 1A, Fig. S2A-C). Gene specific CRISPR/Cas9-editing was further confirmed by RNAi-mediated depletion of endogenous LC3 or GABARAP proteins in the corresponding HA-tagged hATG8 cell lines (Fig. 1B, Fig. S2D-F). Consistently, confocal microscopy of GABARAPL2^{endoHA} cells showed a substantially decreased HA immunolabeling upon knockdown of GABARAPL2 (Fig. 1C). Next, we examined the integrity of the tagged LC3/GABARAP proteins by monitoring their conjugation to PE in response to treatment with small molecule inhibitors which either increase lipidation (Torin1), block autophagosomal degradation (Bafilomycin A1 (BafA1)) or prevent ATG8-PE conjugate formation (ATG7 inhibitor). As expected, GABARAPL2^{endoHA}, GABARAP^{endoHA} and LC3B^{endoHA} cell lines showed treatment-specific lipidation levels of the respective tagged hATG8 protein (Fig. 1D; Fig. S2G,I). We also detected lipidated GABARAPL1, though in a manner that was independent from induction or blockage of autophagy (Fig. 3E). However, as expected autophagy induction robustly decreased HA-GABARAPL1 protein levels in GABARAPL1^{endoHA} cells while blockage of autophagosomal degradation led to the opposite phenotype (Fig. S2H). Next, we analyzed the subcellular distribution of one of the HA-tagged hATG8 proteins (i.e. GABARAPL2) in basal and autophagy-modulating conditions using confocal microscopy. In GABARAPL2^{endoHA} cells, HA-GABARAPL2 was indeed found to colocalize with the autophagosomal and -lysosomal markers p62, LC3B and LAMP1 and this colocalization increased upon combination treatment with Torin1 and BafA1 (Fig. 1E-G). Together, we successfully engineered cell lines to carry epitope tagged hATG8 family members which retain their functionality.

Mapping the endogenous GABARAPL2 interactome

Next, we selected GABARAPL2^{endoHA} cells for a proof-of-principle immunoprecipitation (IP) followed by mass spectrometric (MS) analysis to identify new candidate binding partners of a hATG8 family member at endogenous levels. To distinguish between candidates that bind preferentially to PE-conjugated versus unconjugated GABARAPL2 we treated stable isotope labeling with amino acids in cell culture (SILAC)-labeled GABARAPL2^{endoHA} cells with Torin1 and BafA1 (light) or ATG7 inhibitor (heavy). Equal amounts of heavy and light SILAC cells were mixed, lysed and subjected to an HA-IP. Immune complexes were eluted and size separated by gel electrophoresis followed by in-gel tryptic digest, peptide extraction and desalting prior to analysis by liquid chromatography tandem MS. SILAC labeled parental HeLa cells differentially treated with Torin1/BafA1 or ATG7 inhibitor served as a negative control. In duplicate experiments, we identified a total of 168 proteins whose abundances in GABARAPL2 immunoprecipitates were altered by at least 2.8-fold (log_2 SILAC ratio ≥1.5 or ≤-1.5) in response to modulation of the GABARAPL2 conjugation status (Fig. 2A). Among these regulated proteins were well-characterized hATG8 binding proteins such as ATG7, CCPG1 and SQSTM1 (also known as p62) as well as several candidate interactors of LC3 and GABARAP proteins previously found in large-scale screening efforts such as the mitochondrial outer membrane protein VDAC1, the nucleoprotein AHNAK2, the translation initiation factor EIF4G1 and the small GTPase IRGQ (Ewing et al., 2007, Rolland et al., 2014) (Fig. 2A). In addition, a number of known hATG8 binding proteins including UBA5, HADHA, HADHB, RB1CC1, TRIM21 and IPO5 was found to bind GABARAPL2 independent of its lipidation status since these proteins did not display substantial changes in their SILAC ratios.

ACSL3 is a novel binding partner of GABARAPL2

Since functional annotation analysis using DAVID revealed ‘fatty acid metabolism’ as a term previously not associated with LC3/GABARAP-interacting proteins (Fig. S2J), we focused on the proteins found in this category. In particular, the long-chain-fatty-acid-CoA ligase 3 (ACLS3) attracted our attention as it was the only ER-localized protein among these candidates. To validate ACSL3 as novel GABARAPL2 interacting protein, we performed HA-IPs on lysates derived from parental and GABARAPL2^{endoHA} cells which were either transiently transfected with ACSL3-myc, myc-p62 or -ATG7 or left untreated. Notably, p62 and ATG7 served as positive controls. Immunoblotting with epitope tag- and gene-specific antibodies revealed that overexpressed and endogenous p62 and ATG7 as well as ACSL3 associated

with endogenous GABARAPL2 (Fig. 2B,C). Thus, these results indicate that our hATG8^{endoHA} cells are indeed valuable tools to examine the LC3 and GABARAP interactome at endogenous levels and to identify novel binding partners such as ACSL3.

GABARAPL2 is stabilized by ACSL3

Since GABARAPL2 is involved in autophagic cargo engulfment (Schaaf et al., 2016), we tested whether ACSL3 is an autophagy substrate or serves as selective autophagy receptor. However, stimulation of GABARAPL2^{endoHA} cells with Torin1, BafA1, a combination of both or with ATG7 inhibitor showed that ACSL3 protein levels did not change upon autophagy induction or blockage (Fig. 3A). Likewise, depletion of GABARAPL2 had no effects on ACSL3 abundance (Fig. 3B). Thus, these results indicate that ACSL3 is neither a substrate nor a receptor of autophagy under these conditions. Next, we examined the effects of ACSL3 knockdown on GABARAPL2. Treatment of GABARAPL2^{endoHA} cells with two different ACSL3 siRNAs showed a significant decrease of GABARAPL2 protein levels (Fig. 3C). To rule out that this phenotype is due to a global perturbation of the ER, we probed for the integrity of this organelle in cells depleted of ACSL3 using immunolabeling with Calnexin and the ER exit site marker SEC13. However, neither the meshwork appearance nor the exist sites of the ER showed any overt alterations (Fig. S3A,B). Given the high structural and functional similarity between LC3 and GABARAP family members we addressed whether ACSL3 depletion likewise impacts on the protein abundance of the other hATG8 family members. Unexpectedly, ACSL3 knockdown experiments in GABARAP^{endoHA}, GABARAPL1^{endoHA} and LC3B^{endoHA} cells did not show any significant reduction in the respective HA-tagged hATG8 proteins (Fig. 3D-F). In contrast, we found that LC3B protein levels significantly increased upon ACSL3 depletion (Fig. 3F), suggesting that reduced GABARAPL2 levels might be compensated by increased expression of LC3B. Intriguingly, we observed that GABARAPL2 protein levels are restored in RNAi-treated GABARAPL2^{endoHA} cells treated with BafA1 to block autophagosomal degradation but not with the proteasome inhibitor Bortezomib (Btz) (Fig. 3G). Together, these results indicate that ACSL3 is not degraded by autophagy but rather serves as a specific stabilizing factor of GABARAPL2 at the ER.

GABARAPL2 localizes with ACSL3 at the ER

ACSL3 is one of five acyl-CoA synthetases and catalysis the conjugation of CoA to long chain fatty acids to form acyl-CoA (Soupene and Kuypers, 2008). Besides ACSL3 was found to regulate the formation, the size and the copy number of lipid droplets (Fujimoto et al., 2007,

Kassan et al., 2013). Consistent with its cellular role, ACSL3 is inserted with its N-terminal helix region midway into the lipid bilayer of the ER membrane or integrated into the monolayer of lipid droplets (LD) while its C-terminal part encompassing the AMP-binding domain is facing to the cytoplasm (Brasaemle et al., 2004, Ingelmo-Torres et al., 2009, Poppelreuther et al., 2012). To further validate the GABARAPL2-ACSL3 interaction, we sought to examine the subcellular localization of both proteins by confocal microscopy. However, as there were no suitable antibodies for immunofluorescence staining of endogenous ACSL3, we gene-edited GABARAPL2^{endoHA} cells to express ACSL3 tagged at its C-terminus with NeonGreen (Fig. S1A,C). Immunoblot analysis of these newly established GABARAPL2^{endoHA}/ACSL3^{endoNeonGreen} cells in comparison with GABARAPL2^{endoHA} and parental Hela cells transfected with TOMM20-NeonGreen confirmed the correct size of the ACSL3-NeonGreen fusion (approximately 106 kDa; ACSL3 80 kDa + NeonGreen 26 kDa) (Fig. 4A). Colocalization of ACSL3-NeonGreen with the ER-membrane localized chaperone Calnexin demonstrated that the NeonGreen tag did not interfere with the ER localization of ACSL3 (Fig. 4B). As ACSL3 is essential for LD formation, we tested whether the ACSL3-NeonGreen chimera is fully functional. Thereto, GABARAPL2^{endoHA}/ ACSL3^{endoNeonGreen} cells were treated with oleic acid to induce LD formation or EtOH as control prior to fixation and labeling of phospholipids and neutral lipids. Confocal microscopy showed a clear colocalization of ACSL3 with phospholipids and neutral lipids in control cells while ACSL3 redistributed in the phospholipid monolayer of LDs when cells were treated with oleic acid for 24 hrs (Fig. 4C). Next, we analyzed fixed and HA-immunolabeled GABARAPL2^{endoHA}/ACSL3^{endoNeonGreen} cells by confocal microscopy and super-resolution radial fluctuations (SRRF) imaging. Consistent with our biochemical experiment, we observed partial colocalization of endogenous GABARAPL2 and ACSL3 (Fig. 4D). Together, these results show that NeonGreen tagged ACSL3 is correctly localized at the ER membrane, integrates into the monolayer of LDs upon free fatty acid treatment and associates with GABARAPL2 at the ER.

ACSL3 binds GABARAPL2 in a LIR-dependent manner

Interaction between hATG8 proteins and their binding partners involves an ATG8 family-interacting motif (AIM; also known as LC3-interacting region (LIR)) in the hATG8 interactors and the LIR-docking site (LDS) in LC3 and GABARAP proteins (Noda et al., 2008, Pankiv et al., 2007, Rogov et al., 2014). Amino acid sequence analysis of ACSL3 with iLIR (Kalvari et al., 2014) and manual inspection revealed four potential LIRs (LIR-1: 65-71, LIR-2: 135-140, LIR-3: 589-594, LIR-4: 643-648) (Fig. 5A). To determine whether ACSL3 employs at least one

of these sites to bind GABARAPL2 we performed binding experiments with purified GST-tagged wild-type and a LIR-binding deficient GABARAPL2 mutant in which the relevant amino acids of the LDS were replaced with alanine (i.e. Y49A/L50A). These two GABARAPL2 variants were incubated with lysates derived from HeLa cells stably expressing full-length ACSL3 or two fragments thereof. While the first fragment spanned residues 1-85 and included the ER membrane-binding domain and LIR-1, the second fragment ranged from residues 86-718 and contained the AMP binding site, LIR-2-4 (Fig. 5A). Immunoblot analysis of the pulldown assay showed binding of wild-type GABARAPL2 to full-length ACSL3 and both of its fragments (Fig. 5B), indicating that ACSL3 contains at least two distinct binding sites for GABARAPL2. Intriguingly, GABARAPL2 lacking a functional LDS did not interact with ACSL3 86-718 while it retained binding to the wild-type ACSL3 and fragment 1-85 (Fig 5B). This suggests that GABARAPL2 employs its LDS to bind to a LIR within residues 86-718 of ACSL3 while GABARAPL2 seem to employ a different binding site to interact with a motif in the preceding ACSL3 sequence. To start dissecting the relevance of our binding model for the recruitment of GABARAPL2 to ACSL3 at the ER, we subjected HeLa cells stably expressing wild-type or LIR-binding deficient GABARAPL2 to subcellular fractionation using differential centrifugation. Consistent with our finding that ACSL3 binds GABARAPL2 in a LIR-dependent manner, immunoblot analysis revealed that wild-type GABARAPL2 is found in the ER fraction but GABARAPL2 ΔLDS fail to cofractionate with the ER (Fig. 5C, Fig. S4B). Taken together these results indicate that the ACSL3-GABARAPL2 interaction involves more than one binding motif and binding site in GABARAPL2 and ACSL3 and that LIR-dependent ACSL3 binding is required for the ER recruitment of GABARAPL2.

ACSL3 anchors UBA5 to the ER membrane

To better understand the biological significance of the GABARAPL2-ACSL3 interaction, we turned our attention to known GABARAPL2 binding proteins and in particular to the ubiquitin-like modifier activating enzyme 5 (UBA5) (Komatsu et al., 2004), which was recently shown to be recruited to the ER membrane in a GABARAPL2-dependent manner (Huber et al., 2019). By subjecting lysates derived from parental and GABARAPL2^{endoHA} cells that were transiently transfected with myc-UBA5 or left untreated to HA-IPs, we confirmed the GABARAPL2-UBA5 interaction (Fig. 6A) and demonstrated that it occurs at endogenous levels (Fig. 6B). Since ACSL3 binds GABARAPL2 at the ER membrane, we investigated whether ACSL3 also colocalizes with UBA5. Indeed, immunolabeling of fixed GABARAPL2^{endoHA}/ACSL3^{endoNeonGreen} cells with an anti-UBA5 antibody followed by SRRF imaging showed partially colocalization of UBA5 and ACSL3 (Fig. 6C). Moreover, when we labeled GABARAPL2^{endoHA}/ACSL3^{endoNeonGreen}

cells with anti-UBA5 and anti-HA antibodies we also observed triple localization of ACSL3, GABARAPL2 and UBA5 (Fig. 6D). Next, we examined the effect of GABARAPL2 depletion on the ACSL3-UBA5 interaction. Thereto, we transfected HeLa cells stably overexpressing ACSL3-HA with myc-UBA5 and a siRNA against GABARAPL2 or a non-targeting control followed by HA-IP. Consistent with the notion that GABARAPL2 recruits UBA5 to ACSL3, we observed a clear reduction of UBA5 levels in ACLS3 immunoprecipitates upon GABARAPL2 knockdown (Fig. 6E). Lastly, we asked whether the ACSL3-UBA5 interaction is modulated by lipid stress. To address this question, we performed myc-IPs on lysates derived from myc-UBA5-transfected mock or ACSL3-HA expressing HeLa cells that were grown in the absence and presence of oleic acid. Remarkably, we found that UBA5 associates with ACSL3 independent of its activity during LD formation (Fig. 6F). Overall, these results suggest that ACSL3, GABARAPL2 and UBA5 form a complex at the ER membrane in dependency of GABARAPL2.

ACSL3 regulates ufmylation pathway components

Since we found that ACSL3 stabilizes GABARAPL2, we investigated whether ACSL3 depletion has similar effects on UBA5 protein abundance. For this purpose, GABARAPL2^{endoHA} cells were transfected with siRNA against ACSL3 or a non-targeting control and grown in the absence or presence of BafA1 or Btz. Indeed, we observed that protein levels of UBA5 decreased upon ACSL3 depletion but they were not restored by blockage of autophagosomal or proteasomal degradation (Fig. 7A,B). While depletion of GABARAPL2 had no effects on UBA5 protein levels (Fig. 3B). This supports the notion that UBA5 and GABARAPL2 form a functional unit which is regulated by ACSL3. UBA5 is part of the conjugation system, termed ufmylation, that covalently attaches the ubiquitin-like protein ubiquitin fold modifier 1 (UFM1) to target proteins through an E1-E2-E3 multienzyme cascade. The E1-like enzyme UBA5 activates UFM1 by forming a thioester bond between its active site and the exposed C-terminal glycine of UFM1 (Komatsu et al., 2004). The UFM1-conjugating enzyme 1 (UFC1) then transfers UFM1 from UBA5 to the UFM1-protein ligase 1 (UFL1) which mediates the attachment to target proteins (Komatsu et al., 2004, Tatsumi et al., 2010). While UFC1 is cytosolic, the ER-membrane bound protein DDRGK1 anchors UFL1 to the ER membrane (Wu et al., 2010) and is reported to be one of the few known ufmylation targets besides RPL26 (Walczak et al., 2019), RPN1 (Liang et al., 2019) and ASC1 (Yoo et al., 2014) (Tatsumi et al., 2010). While the consequences of ufmylation remains poorly understood at the mechanistic level, the UFM1 conjugation pathway has been linked to the ER stress response (Lemaire et al., 2011, Zhang et al., 2012), erythrocyte differentiation (Cai et al., 2015, Tatsumi et al., 2011),

cellular homeostasis (Zhang et al., 2015) and breast cancer progression (Yoo et al., 2014). Since the stability of UBA5 and its ER-recruiting factor GABARAPL2 was controlled by ACSL3, we probed whether it also regulates the abundance of the other proteins in the ufmylation cascade. Knockdown experiments revealed that the protein levels of UFL1 and DDRGK1 were significantly decreased upon ACSL3 depletion while the abundance of UFC1 was significantly increased. Conjugated UFM1 was largely unchanged (Fig. 7A,B, Fig. S4C). The observation that the protein levels of UBA5, UFL1 and DDRGK1 were not restored by blockage of autophagy or the proteasome (Fig. 7A,B) indicates that these ufmylation factors are most likely regulated at the transcriptional level. Together, this suggest that ACSL3 not only anchors UBA5 but might act as novel regulator of the ufmylation cascade.

LDs regulate UFM1 conjugation and ER-phagy

The finding that the LD biogenesis factor ACSL3 stabilizes several components of the UFM1 conjugation pathway raises the question whether LD biogenesis and ufmylation are functionally coupled. To test this hypothesis, we monitored the ufmylation pathway in response to induction of LD formation in GABARAPL2^{endoHA} cells grown in the absence and presence of oleic acid for 0.5, 4 and 8 hrs, respectively. While UBA5 levels significantly decreased in the course of 8 hrs oleic acid treatment, there was no effect on UFC1 (Fig. 7C,D). In contrast, the protein levels of DDRGK1 and UFL1 both decreased in the first 4 hrs of incubation with oleic acid but after 8 hrs at least DDRGK1 levels were almost restored (Fig. 7C,D). Interestingly, we detected significantly more conjugated UFM1 (~35 kDa) after 4 hrs of oleic acid incubation (Fig. S4D) which might be due to altered ufmylation and de-ufmyltion dynamics. Given that LD formation induced a substantial suppression of several ufmylation components and that these components was recently shown to be required for starvation-induced, ER sheet-targeting selective autophagy (Liang et al., 2019), we examined whether induction of LD blocks this ER-phagy pathway. Thereto, we employed the recent developed ER-autophagy tandem reporter system which allows the quantification of reticulolysosomes (Liang et al., 2018). Briefly, HeLa cells were transfected with mCherry-eGFP-RAMP4 and starved with EBSS for 8 hrs in combination with either EtOH or oleic acid. As expected, we observed a robust decrease in the numbers of red-only puncta which indicates reduced reticulolysosomes and hence an inhibition of ER-phagy (Fig. 8A,B). Together, these results indicate that the ufmylation cascade is differentially regulated during induction of LD and that the ACSL3-GABARAPL2-UBA5 axis plays an important part in this regulation.

Discussion

In this study, we identified the ER-associated protein ACSL3 as novel binding partner of GABARAPL2 and UBA5 using a CRISPR/Cas9 generated GABARAPL2^{endoHA} cell line. Furthermore, we provide evidences for the regulation of ufmylation through ACSL3 and LD biogenesis.

In our interactome screen with endogenously tagged GABARAPL2 we found ACSL3, which we confirmed as GABARAPL2 interactor by immunoprecipitations, GST pulldowns and SRRF imaging. Moreover, our data suggest, that this interaction is mediated by a LIR and one additional binding motif in ACSL3. By using GABARAPL2 LIR-binding deficient mutants as well as N- and C-terminal ACSL3 fragments we narrowed down the LIR in ACSL3 within the amino acids 86-718, thereby excluding candidate LIR-1. Given that candidate LIR-2 is localized within the AMP-binding domain of ACSL3 and therefore unlikely accessible, candidate LIR-3 or -4 might mediate the binding to the LDS of GABARAPL2 (Fig. S4A). In addition, our binding studies indicate a GABARAPL2 LDS-independent binding motif within residues 1-85 of ACSL3. In addition to the LIR/LDS pairing, Marshall and colleagues recently reported an alternative hATG8 interaction modus in which binding partners employ a ubiquitin-interacting motif (UIM) to bind to an UIM-docking site (UDS) in LC3 and GABARAP proteins (Marshall et al., 2015). According to the UIM consensus sequence (Marshall and Vierstra, 2019) we indeed found a potential UIM (amino acids 73-81) in ACSL3 by manual sequence inspection (Fig. S4A). However, this candidate UIM is reversed in its sequence similar to inverted SUMO interaction motifs (Matic et al., 2010). Whether and how this UIM bind to GABARAPL2's UDS remains to be structurally determined. Importantly, our subcellular fractionation assay revealed that GABARAPL2 recruitment to the ER membrane is dependent on the LIR of ACSL3 as the LDS GABARAPL2 mutant was dramatically reduced in the ER membrane fractions compared to wild-type GABARAPL2.

GABARAP proteins were shown to mediate ER recruitment of UBA5 to bring it in close proximity to the membrane bound UFM1 E3 enzyme complex composed of UFL1, DDRGK1 and CDK5R3, thereby facilitating ufmylation (Huber et al., 2019). However, since GABARAPs are not known to be conjugated to PE at the ER, the molecular basis of this recruitment process was not clear. Here, we provided evidence that ACSL3 function to anchor UBA5 at the ER membrane. Given that UBA5 employs an atypical LIR to bind both GABARAPL2 and UFM1 and that the latter is able to outcompete GABARAPL2 binding of UBA5 *in vitro* (Habisov et al., 2016), it is tempting to speculate that GABARAPL2 interacts with UBA5 until UFM1 conjugation is triggered. In this scenario, GABARAPL2 is a recruiting factor that hands UBA5

over to ACSL3 (Fig. 8C). However, the binding mode of ACSL3 and UBA5 remains to be explored.

While targets of ufmylation are still largely unknown, three of the known UFM1-modified proteins are linked to the ER. Firstly, UFM1 conjugation of DDRGK1 is essential for the stabilization of the serine/threonine-protein kinase/endoribonuclease IRE1 (inositol-requiring enzyme 1) (Liu et al., 2017, Yoo et al., 2014). Secondly, it was shown that the 60S ribosomal protein L26 (RPL26) is exclusively ufmylated and de-ufmylated at the ER membrane (Walczak et al., 2019). Thirdly, Ribophorin1 (RPN1), an ER transmembrane protein and part of the oligosaccharyltransferase complex, is ufmylated in a DDRGK1-dependent manner (Liang et al., 2019, Kelleher et al., 1992). Overall, emerging evidence points to a role of the UFM1 conjugation system as regulator of ER homeostasis, ER stress response and ER remodeling. Disruption of protein folding and accumulation of unfolded proteins in the ER are hallmarks of ER stress which leads to the induction of the unfolded protein response (UPR) via one of these three key factors: IRE1, PKR-like ER protein kinase (PERK) or activating transcription factor 6 (ATF6). Protein degradation, reduction of protein synthesis and enlargement of the ER capacity are part of the UPR (Karagoz et al., 2019). In different cell lines and animal models, it was reported that ufmylation is upregulated via IRE1 or PERK upon ER stress, while depletion of ufmylation components induce the UPR (Gerakis et al., 2019, Lemaire et al., 2011, Zhang et al., 2015, Zhang et al., 2012, Zhu et al., 2019). Upon re-established ER homeostasis, ufmylation coordinates the elimination of extended ER membranes through ER-phagy (Liang et al., 2019, DeJesus et al., 2016).

In our present study, we identified LD formation stimulated by oleic acid treatment as novel regulator of ufmylation. LD biogenesis starts with lens formation, an accumulation of neutral lipids between the ER membrane leaflets until LDs eventually bud from the ER. The hydrophobic neutral lipid core of a LD is surrounded by a phospholipid monolayer with the origin of the outer ER membrane leaflet (Henne et al., 2018). ACSL3 was identified as LD associated protein and essential for LD biogenesis, expansion and maturation (Fujimoto et al., 2004, Kassan et al., 2013). During initiation of LD biogenesis ACSL3 is translocated and concentrated to pre-LDs to drive LD expansion by mediating acyl-CoA synthesis. However, cells with enzymatically inactive ACSL3 are still able to form LDs, suggesting additional functions of ACSL3 in LD biogenesis (Kassan et al., 2013, Kimura et al., 2018). Induction of LD formation induced by oleic acid which requires ACSL3 resulted in a reduction of UBA5, UFL1 and DDRGK1 protein levels and thus potentially shut down of UFM1 conjugation (Fig. 7C,D, Fig. 8C). Interestingly, depletion of ACSL3 led to a similar phenotype with regard to these three ufmylation components. Together, these results suggest that ACSL3 regulates UBA5, DDRGK1 and UFL1 protein levels and therefore ufmylation (Fig. 8C). The observation

that inhibition of proteasomal or lysosomal degradation did not rescue this phenotype suggests that these components of the ufmylation machinery are probably downregulated at the transcriptional level. To what extend this involves one of the three UPR factors IRE1, PERK or ATF6 remains to be examined. Consisting with the recent finding that ER-phagy is blocked by inhibition of the interaction between DDRGK1 and UFL1 (Liang et al., 2019), we observed that LD biogenesis inhibits the remodeling of ER membranes by ER-phagy. While DDRGK1 protein levels are restored 8 hrs after induction of LD formation it needs to be further investigated when UFL1 protein levels are reestablished and therefore ER-phagy is restored.

Collectively, these findings underline the potential of our CRISPR/Cas9 gene-edited cell lines to uncover novel cellular pathways involving hATG8 family members without the need of overexpression systems, thereby complementing the recently generated LC3 and GABARAP knockout cell lines (Nguyen et al., 2016). Together with the LC3C^{endoHA} cell line that we previously reported (Le Guerroue et al., 2017), this cellular resource circumvents the drawback of unspecific LC3 and GABARAP antibodies and hence will greatly facilitate the functional dissection of individual hATG8 proteins.

Material and Methods

Cell culture and treatments

HeLa cell lines were cultured in Dulbecco's modified Eagle's medium (DMEM) + GlutaMAX-I (Gibco) supplemented with 10 % fetal bovine serum (FBS) and 1mM sodium pyruvate (Gibco) and grown at 37° C and 5 % CO_2. For SILAC mass spectrometry, cells were grown in lysine- and arginine-free DMEM (Gibco) supplemented with 10 % dialyzed FBS, 2 mM glutamine (Gibco), 1 mM sodium pyruvate (Gibco) and 146 mg/ml light (K0, Sigma) or heavy L-lysine (K8, Cambridge Isotope Laboratories) and 84 mg/ml light (R0, Sigma) or heavy L-arginine (R10, Cambridge Isotope Laboratories). SILAC labeled cells were counted after harvesting, mixed 1:1 and stored at -80° C. For selection Puromycin (2 µg/ml) or Blasticidine (4 µg/ml) was added to the growth medium. The following reagents were used for treatments: oleic acid (EMD Millipore, 4954, 600 µm in EtOH, 0.5, 4, 8 or 24 hrs), Bafilomycin A1 (Biomol, Cay11038-1, 200 nM in DMSO, 2 hrs), Torin 1 (Tocris, 4247, 250 nM in DMSO, 2 hrs), Bortezomib (LC Labs B-1408, 1 µM in PBS, 8 hrs), ATG7 inhibitor (Takeda ML00792183, 1 µM in DMSO, 24 hrs), EBSS (Sigma E2888, 8 hrs), Doxycycline hyclate (Sigma D9891, 4 µg/ml, 24 hrs).

Plasmids and stable cell lines

attB flanked ORFs, generated by PCR were cloned into the Gateway entry vector pDONR233. ORFs from pDONR233 constructs were introduced into one of the following destination vectors using recombination cloning: pHAGE-N-Flag-HA, pHAGE-C-FLAG-HA, pET-60-DEST, pEZYmyc-HIS (Addgene, #18701) or pDEST-myc. Stable HA-GABARAPL2 and ACSL3-HA expressing cells were generate by lentiviral transduction followed selection with 2 µg/ml Puromycin. pEZY and pDEST constructs were used for transient expression in cells (see transfection).

Site directed mutagenesis

For site directed mutagenesis, primers were designed with Quick Change Primer Design software (Agilent Technologies). First, forward and reverse primers were used in individual PCR reactions using KOD Hot Start polymerase (Merck Millipore), according to the instruction of the manufacturer, with the appropriate pDONOR-ORF plasmid as template. In a second step, PCR reactions were combined and plasmids with the mutated ORF was generated through a second round of PCR. The obtained PCR mixture was purified with QIAquick PCR Purification Kit (Qiagen, 28104) and mutated plasmids were amplified in E. coli. Mutagenesis was verified by sequencing the purified plasmid.

Genome editing

The N-terminal HA-tagged hATG8 cell lines were generated with homology PCR templates containing 87 bp of GABARAP/GABARAPL1/GABARAPL2/LC3B-5'UTR including the start codon followed by the Blasticidine resistance gene, P2A, HA and 92bp downstream of the start codon of the corresponding hATG8 gene. For the C-terminal ACSL3-NeonGreen cell line, we used a homology PCR template containing 75 bp of the last exon of ACSL3, the NeonGreen ORF (Allele Biotech), T2A and the Blasticidine resistance gene ending with 84 bp downstream of the last exon of ACSL3. sgRNAs for hATG8s and ACSL3, designed with the online design tool from the Broad Institute (https://portals.broadinstitute.org/gpp/public/analysis-tools/sgrna-design) were clone into BSbI digested px330 (Addgene #42230), a SpCas9 expressing plasmid (sgRNA: GABARAP: GGAGGATGAAGTTCGTGTAC, GABARAPL1: TGCGGTGCATCATGAAGTTC, GABARAPL2: CCATGAAGTGGATGTTCAAG, LC3B: AGATCCCTGCACCATGCCGT,

ACSL3: AGAAAATAATTATTCTCTTC). HeLa cells were seeded in a 6-well plate and transfected with Lipofectamin 2000 according to the manufacturer's instructions with sgRNA and corresponding homology PCR template. 48 hrs later cells were selected with 4 µg/ml Blasticidine and subjected to single cell selection in 96-well plates. Cells with mNeonGreen insertion were FACS sorted. Correct introduction of the tag was verified by PCR and sequencing.

Antibodies and dyes

For immunoblotting the following primary antibodies were used at a concentration of 1:1000 in 5 % milk-TBS-T or 5 % BSA-TBS-T or 0.2 % I-Block-TBS-T: ACSL3 (Santa Cruz, sc-166374), alpha-Tubulin (Abcam, ab64503), ATG7 (Cell Signaling, 8558), Calnexin (Cell Signaling, 2433), c-myc (Bethyl, A190-104A), COXIV (Cell Signaling, 4850), DDRGK1 (Sigma, HPA013373), GM130 (Abcam, ab52649), HA (Cell Signaling, 3724S/Biolegend, 901501), LaminA/C (Abcam, ab108595), mNeonGreen (Chromotek, 32F6), PCNA (Santa Cruz, sc-7907), p62 (MBL, PM045/BD, 610832), UBA5 (Proteintech, 12093-1-AP/Sigma, HPA017235), UFC1 (Proteintech, 15783-1-AP), UFL1 (Abcam, ab226216), UFM1 (Abcam, ab109305) or at a concentration of 1:100 in 5 % milk-TBS-T: c-myc (Monoclonal Antibody Core Facility, Helmholtz Zentrum Munich, 9E1, rat IgG1), c-myc (Monoclonal Antibody Core Facility, Helmholtz Zentrum Munich, 9E10, mouse IgG). As secondary antibodies we used horseradish peroxidase coupled anti-mouse (Promega, W402B), anti-rabbit (Promega, W401B) and anti-goat (Dianova, 705035003) antibodies at a concentration of 1:10 000 and anti-rat IgG1 (Monoclonal Antibody Core Facility, Helmholtz Zentrum Munich) antibody at a concentration of 1:100 in 1 % milk-TBS-T or 1 % BSA-TBS-T or 0.2 % iBlock-TBS-T. The following primary antibodies and lipid stains were used for immunofluorescence in 0.1 % BSA-PBS: Calnexin (Stressgen, SPA-860, 1:100), HA (Roche, 11867423001, 1:50), LAMP1 (DSHB, H4A3, 1:50), LC3 (MBL, PM036, 1:500), p62 (BD, 610832, 1:500), SEC13 (Novus, AF9055-100, 1:300), HCS LipidTOX™ Red Phospholipidosis Detection Reagent (Thermo Scientific, H34351, 1:1000) and HCS LipidTOX™ Deep Red Neutral Lipid Stain (Thermo Scientific, H34477, 1:500). The following fluorophore conjugated secondary antibodies from Thermo Fisher were use at a concentration of 1:1000 in 0.1 % BSA-PBS: anti-mouse IgG Alexa Fluor 488 (A-11001), anti-rabbit IgG Alexa Fluor 488 (A-11008) and anti-rat IgG Alexa Fluor 647 (A-21247).

Transfection

For siRNA knockdowns, cells were reversely transfected with Lipofectamine RNAiMax (Thermo Fisher Scientific) according to the manufacturer's guidance with 30 nM of the following siRNAs from Dharmacon/Horizon Discovery and harvested 72 hrs after transfection: sictrl UGGUUUACAUGUUUUCCUA, siACSL3#1 UAACUGAACUAGCUCGAAA, siACSL3#2: GCAGUAAUCAUGUACACAA, siGABARAP GGUCAGUUCUACUUCUUGA, siGABARAPL1 GAAGAAAUAUCCGGACAGG, siGABARAPL2 GCUCAGUUCAUGUGGAUCA, siLC3B GUAGAAGAUGUCCGACUUA. Plasmids were transiently transfected with Lipofectamine 2000 (Thermo Fisher Scientific) according to the instruction of the manufacturer or with 10 mM PEI (Polyethylenimine) and cells were collected after 48 hrs.

Immunoblotting

Cell were lysed in RIPA (50 mM Tris-HCl [pH 7.4], 150 mM NaCl, 0.5 % sodium desoxycholate, 1 % NP-40, 0.1 % SDS, 1x EDTA-free protease inhibitor (Roche), 1x phosphatase inhibitor (Roche)) for 30 min. After elimination of cell debris by centrifugation, proteins were diluted with 3x loading buffer (200 mM Tris-HCl [pH 6.8], 6 % SDS, 20 % Glycerol, 0.1 g/ml DTT, 0.1 mg Bromophenol blue) and boiled at 95°C. Proteins were size separated by SDS-PAGE with self-casted 8 %, 10 %, 12 % and 15 % gels followed by protein transfer onto nitrocellulose membranes (GE Healthcare Life Sciences, 0.45 µm). For better visibility of endogenous HA-hATG8s membranes were boiled for 5 min in PBS after protein transfer. For GST pulldowns, equal sample loading was confirmed with 5 min Ponceau staining (0.2 % Ponceau S, 3 % acetic acid) followed by a 10 min TBS-T washing step. Blots were blocked in TBS-T (20 mM Tris, 150 mM NaCl, 0.1 % Tween-20) supplemented with 5 % low fat milk (Roth) or 5 % BSA (Albumin from bovin serum, Sigma) or 0.2 % I-Block protein based blocking reagent (Thermo Fisher) for 1 hr. Primary antibodies were incubated overnight followed by several wash steps with TBS-T and incubation with secondary antibodies for 1 hr at room temperature. After repeated washing, immunoblots were analyzed with Western Lightning Plus ECL (Perkin Elmer).

Immunofluorescence

All steps were carried out at room temperature. Cells growing on glass coverslips in 12-well plates were fixed with 4 % paraformaldehyde in PBS for 15 min followed by permeabilization

with 0,1 % Trition-X-100 in PBS or 0,1 % Saponin in PBS for 15 min and 1 hr blocking in 1 % BSA-PBS. First and secondary antibody incubation was done sequentially for 1 hr at room temperature in 0.1 % BSA-PBS followed by mounting of the coverslips with ProlongGold Antifade with Dapi (Thermo Fisher). In between each step, cells were washed several times with PBS. Cells were imaged with a LSM 800 Carl Zeiss microscope using 63x oil-immersion objective and ZEN blue edition software and analyses with ImageJ (version 1.52).

Sample preparation for SRRF imaging

For super-resolution radial fluctuations (SRRF; ref. PMID: 29852248) imaging, GABARAPL2^{endoHA}/ACSL3^{endoNeonGreen} cells were seeded on 18 mm diameter coverslips at a density of 2x10^5 per 35 mm dish. Following overnight incubation, cells were fixed with 4 % PFA for 15 min at room temperature, washed three times with 1x PBS followed by a 5 min additional washing with 50 mM NH_4Cl. Permeabilization was performed for 5 min with 0.5 % Triton X-100 and blocking for 40 min in 1 % BSA. Following antibodies were used at room temperature in 1 % BSA for 1 hr. Rabbit polyclonal anti-Calnexin (Abcam, ab22595, 1:500), mouse monoclonal anti-HA (Sigma, H9658, 1:500) and rabbit polyclonal anti-UBA5 (PTGLab, 12093-a-AP, 1:250).

Acquisition of SRRF images

Confocal microscopy imaging of immunostained HeLa cells was performed on Andor Dragonfly spinning disk using a Nikon Ti2 inverted optical microscope (60x TIRF objective (Plan-APOCHROMAT 60 × /1.49 Oil)). Fluorescence was collected with an EMCCD camera (iXon Ultra 888, Andor). Images were acquired using SRRF-Stream mode in Fusion (version 2.1, Andor) with additional 1.5x magnification. Following imaging parameters were used. SRRF Frame count: 150, SRRF Radiality Magnification: 4x, SRRF Ring Radius: 1.4 px, SRRF Temporal Analsysis: Mean and SRRF FPN correction: 75 frames.

Immunoprecipitation

Frozen cell pellets from 4x15 cm cell culture plates for mass spectrometry or 2x10 cm cell culture plate for immunoblotting were lysed in Glycerol buffer (20 mM Tris [pH 7.4], 150 mM NaCl, 5 mM EDTA, 0.5 % Triton-X-100, 10 % Glycerol, 1x protease inhibitor, 1x phosphatase inhibitor) for 30 min at 4° C with end-over-end rotation. Lysates were cleared from cell debris by centrifugation prior to adjustment of protein concentrations between the samples and

overnight immunoprecipitation at 4° C with pre-equilibrated anti-HA-agarose (Sigma) or anti-c-myc-agarose (Thermo fisher). Agarose beads were washed five times with Glycerol buffer followed by elution of proteins with 3x loading buffer and boiling of the samples at 95° C. Samples were then analyzed by SDS-PAGE (self-casted or BioRad's 4-20 % gels) followed by immunoblotting or in-gel tryptic digestion.

Mass spectrometry

SDS-PAGE gel lines were cut in 12 equal size bands, further chopped in smaller pieces and placed in 96 well plates (one band per well). Gel pieces were washed with 50 mM ammonium bicarbonate (ABC)/50 % EtOH buffer followed by dehydration with EtOH, reduction of proteins with 10 mM DTT in 50 mM ABC at 56° C for 1 hr and alkylation of proteins with 55 mM iodacetamide in 50 mM ABC at room temperature for 45 min. Prior to overnight trypsin-digest (12 ng/ul trypsin in 50 mM ABC, Promega) at 37° C, gel pieces were washed and dehydrated as before. Peptide were extracted from gel pieces with 30 % acetonitrile/3 % trifluoroacetic acid (TFA), 70 % acetonitrile and finally 100 % acetonitrile followed by desalting on custom-made C18-stage tips. Using an Easy-nLC1200 liquid chromatography (Thermo Scientific), peptides were loaded onto 75 µm x 15 cm fused silica capillaries (New Objective) packed with C18AQ resin (Reprosil- Pur 120, 1.9 µm, Dr. Maisch HPLC). Peptide mixtures were separated using a gradient of 5 %–33 % acetonitrile in 0.1 % acetic acid over 75 min and detected on an Q Exactive HF mass spectrometer (Thermo Scientific). Dynamic exclusion was enabled for 30 s and singly charged species or species for which a charge could not be assigned were rejected. MS data were processed with MaxQuant (version 1.6.0.1) and analyzed with Perseus (version 1.5.8.4, http://www.coxdocs.org/doku.php?id=perseus:start). IP experiments from GABARAPL2^{endoHA} and control parental HeLa cells were performed in duplicates and triplicates, respectively. Matches to common contaminants, reverse identifications and identifications based only on site-specific modifications were removed prior to further analysis. Log2 heavy/light ratios were calculated. A threshold based on a log2 fold change of greater than 1.5-fold or less than -1.5-fold was chosen so as to focus the data analysis on a smaller set of proteins with the largest alterations in abundance. Additional requirements were at least two MS counts, unique peptides and razor peptides as well as absence in IPs from parental HeLa control cells. For functional annotations, the platform DAVID (https://david.ncifcrf.gov/) was used.

Subcellular fractionation

For isolation of the endoplasmic reticulum the Endoplasmic Reticulum Isolation Kit (Sigma, ER0100) was used and all steps were carried out according to the manufacturer's guidance. Each sample consisted of cells derived from 4x10 cm cell culture plates.

Protein expression and purification

For protein expression and purification, pET-60-DEST plasmids containing wild-type or mutant versions of GABARAPL2 were transformed in Rosetta E. coli. Bacteria were grown in LB medium at 37° C at 200 rpm and induced with 1 mM IPTG when an OD600nm of 0.5-0.6 was reached. After 4 hrs, bacteria were harvested by centrifugation and resuspended in lysis buffer (150 mM NaCl, 50 mM Tris [pH 8.0], 100 µg/ml Lysozyme, 1 mM PMSF, 1mM DTT) and sonified at an amplitude of 50 % for 10 min (30 sec sonification/30 sec break). Lysates were cleared from cell debris by centrifugation and incubated overnight with pre-equilibrated glutathione Sepharose 4B (GE Healthcare) at 4° C with end over end rotation. Glutathione beads were washed with 150 mM NaCl, 50 mM Tris [pH 8.0] and GST-proteins were eluted with 10 mM reduced glutathione in 50 mM Tris [pH 8.0]. GST-proteins were dialyzed overnight in TBS with Slide-A-Lyzer cassettes (Thermo Fisher). Purified GST-proteins were stored at -80° C until further usage.

Pulldown assay

Glutathione Sepharose 4B beads were always freshly coupled prior to pulldown assay. For one reaction, 40 µl pre-equilibrated glutathione beads slurry was couple to an appropriate amount of GST-protein overnight at 4° C with end over end rotation. On the next day protein-coupled glutathione beads were washed with 150 mM NaCl, 50 mM Tris [pH 8.0]. Cells from 2x10 cm cell culture plates per sample were lysed in 600 µl Glycerol buffer for 1 hr. After clearance of cell debrides by centrifugation lysates were precleared for 1 hr at 4° C with pre-equilibrated uncoupled glutathione beads prior to the adjustment of protein concentrations. To ensure equal addition of the different GST-proteins, protein-beads binding was monitored by serial dilutions on Coomassie (0.1 % Brilliant Blue R, 40 % EtOH, 10 % Acetic acid) stained acrylamide gels. Accordingly coupled beads were diluted and 40 µl per sample was added. After overnight incubation at 4° C, beads were washed with Glycerol buffer and boiled for 5 min at 95 ° C.

ER-phagy assay

HeLa cells were seeded on glass coverslips in 12-well plates. The next day, cells were transfected with TETOn-mCherry-GFP-RAMP4 at 500 ng per well with FuGENE® HD transfection reagent (Promega), using manufacturer's recommendations and in the presence of 4 µg/ml doxycycline. After 24 hrs, cells were placed into fresh complete DMEM medium and doxycycline was removed. 40 hrs after initial transfection, cells were starved with EBSS medium for 8 hrs in the presence of either EtOH or oleic acid. Cells were then fixed with 4 % paraformaldehyde in PBS, pH 7.2 at room temperature for 10 min, washed 3x 5 min with PBS, stained with 1/5000 DAPI in the penultimate wash and mounted in Dako fluorescent mounting medium (Dako) onto glass slides. Images were captured with a Nikon A1R TiE confocal microscope using a 100x 1.4 NÅ objective (Nikon Instruments). All confocal images are shown as z-projections of at least 3 z-steps. All quantifications were performed on a minimum of 90 cells across three biological replicates and the standard error of the mean was determined for each data set. Cells were single blind scored for red-only puncta (autolysosomes).

Data availability

The mass spectrometry proteomics data have been deposited to the ProteomeXchange Consortium (http://proteomecentral.proteomexchange.org) via the PRIDE partner repository with the dataset identifier PXD016734.

Statistical analysis

Quantification and statistical analysis were done with imageJ and Phyton (version 3.7). Statistical significance was calculated with Student's t test and data represent ± SEM (standard error of the mean). Statistical analysis of MS data was done with Perseus.

Acknowledgement

We would like to thank Vladimir Rogov, Henrick Riemenschneider, Georg Werner and all members of the Behrends lab for reagents, advice and critical discussion. TetOn-mCherry-eGFP-RAMP4 was a gift from Jacob Corn (Addgene plasmid #109014).

Author contribution

FE performed all experiments except SRRF imaging and ER-phagy assessment which was performed by SP and MDS with advice from HF and SW, respectively. MK provided advice for CRISPR/Cas9 tagging strategy. FE and CB conceived the study and wrote the manuscript.

Competing interests

The authors declare that they have no conflict of interest.

Funding

This work was supported by the Deutsche Forschungsgemeinschaft (German Research Foundation) within the framework of the Munich Cluster for Systems Neurology (EXC2145 - ID 390857198), the Collaborative Research Center 1177 (ID 259130777) and the project grant BE 4685/2-1. Hesso Farhan was supported by grants from the Norwegian Cancer Society (182815, 208015), from the Norwegian Research Council (262717) and from the Rakel go Otto Kr. Bruun legat. A Cancer Research UK Career Development Fellowship to S.W. (C20685/A12825) funded this work. M.D.S. was also funded by a BBSRC grant to S.W. (BB/N000315/1).

References

BAI, H., INOUE, J., KAWANO, T. & INAZAWA, J. 2012. A transcriptional variant of the LC3A gene is involved in autophagy and frequently inactivated in human cancers. *Oncogene,* 31**,** 4397-408.

BAISAMY, L., CAVIN, S., JURISCH, N. & DIVIANI, D. 2009. The ubiquitin-like protein LC3 regulates the Rho-GEF activity of AKAP-Lbc. *J Biol Chem,* 284**,** 28232-42.

BEHRENDS, C., SOWA, M. E., GYGI, S. P. & HARPER, J. W. 2010. Network organization of the human autophagy system. *Nature,* 466**,** 68-76.

BRASAEMLE, D. L., DOLIOS, G., SHAPIRO, L. & WANG, R. 2004. Proteomic analysis of proteins associated with lipid droplets of basal and lipolytically stimulated 3T3-L1 adipocytes. *J Biol Chem,* 279**,** 46835-42.

CAI, Y., PI, W., SIVAPRAKASAM, S., ZHU, X., ZHANG, M., CHEN, J., MAKALA, L., LU, C., WU, J., TENG, Y., PACE, B., TUAN, D., SINGH, N. & LI, H. 2015. UFBP1, a Key Component of the Ufm1 Conjugation System, Is Essential for Ufmylation-Mediated Regulation of Erythroid Development. *PLoS Genet,* 11**,** e1005643.

DEJESUS, R., MORETTI, F., MCALLISTER, G., WANG, Z., BERGMAN, P., LIU, S., FRIAS, E., ALFORD, J., REECE-HOYES, J. S., LINDEMAN, A., KELLIHER, J., RUSS, C., KNEHR, J., CARBONE, W., BEIBEL, M., ROMA, G., NG, A., TALLARICO, J. A., PORTER, J. A., XAVIER, R. J., MICKANIN, C., MURPHY, L. O., HOFFMAN, G. R. & NYFELER, B. 2016. Functional CRISPR screening identifies the ufmylation pathway as a regulator of SQSTM1/p62. *Elife,* 5.

DIKIC, I. & ELAZAR, Z. 2018. Mechanism and medical implications of mammalian autophagy. *Nat Rev Mol Cell Biol,* 19**,** 349-364.

EWING, R. M., CHU, P., ELISMA, F., LI, H., TAYLOR, P., CLIMIE, S., MCBROOM-CERAJEWSKI, L., ROBINSON, M. D., O'CONNOR, L., LI, M., TAYLOR, R., DHARSEE, M., HO, Y., HEILBUT, A., MOORE, L., ZHANG, S., ORNATSKY, O., BUKHMAN, Y. V., ETHIER, M., SHENG, Y., VASILESCU, J., ABU-FARHA, M., LAMBERT, J. P., DUEWEL, H. S., STEWART, II, KUEHL, B., HOGUE, K., COLWILL, K., GLADWISH, K., MUSKAT, B., KINACH, R., ADAMS, S. L., MORAN, M. F., MORIN, G. B., TOPALOGLOU, T. & FIGEYS, D. 2007. Large-scale mapping of human protein-protein interactions by mass spectrometry. *Mol Syst Biol,* 3**,** 89.

FUJIMOTO, Y., ITABE, H., KINOSHITA, T., HOMMA, K. J., ONODUKA, J., MORI, M., YAMAGUCHI, S., MAKITA, M., HIGASHI, Y., YAMASHITA, A. & TAKANO, T. 2007. Involvement of ACSL in local synthesis of neutral lipids in cytoplasmic lipid droplets in human hepatocyte HuH7. *J Lipid Res,* 48**,** 1280-92.

FUJIMOTO, Y., ITABE, H., SAKAI, J., MAKITA, M., NODA, J., MORI, M., HIGASHI, Y., KOJIMA, S. & TAKANO, T. 2004. Identification of major proteins in the lipid droplet-enriched fraction isolated from the human hepatocyte cell line HuH7. *Biochim Biophys Acta,* 1644**,** 47-59.

GENAU, H. M., HUBER, J., BASCHIERI, F., AKUTSU, M., DOTSCH, V., FARHAN, H., ROGOV, V. & BEHRENDS, C. 2015. CUL3-KBTBD6/KBTBD7 ubiquitin ligase cooperates with GABARAP proteins to spatially restrict TIAM1-RAC1 signaling. *Mol Cell,* 57**,** 995-1010.

GERAKIS, Y., QUINTERO, M., LI, H. & HETZ, C. 2019. The UFMylation System in Proteostasis and Beyond. *Trends Cell Biol,* 29**,** 974-986.

HABISOV, S., HUBER, J., ICHIMURA, Y., AKUTSU, M., ROGOVA, N., LOEHR, F., MCEWAN, D. G., JOHANSEN, T., DIKIC, I., DOETSCH, V., KOMATSU, M., ROGOV, V. V. & KIRKIN, V. 2016. Structural and Functional Analysis of a Novel Interaction Motif within UFM1-activating Enzyme 5 (UBA5) Required for Binding to Ubiquitin-like Proteins and Ufmylation. *J Biol Chem,* 291**,** 9025-41.

HENNE, W. M., REESE, M. L. & GOODMAN, J. M. 2018. The assembly of lipid droplets and their roles in challenged cells. *EMBO J,* 37.

HUBER, J., OBATA, M., GRUBER, J., AKUTSU, M., LOHR, F., ROGOVA, N., GUNTERT, P., DIKIC, I., KIRKIN, V., KOMATSU, M., DOTSCH, V. & ROGOV, V. V. 2019. An atypical LIR motif within UBA5 (ubiquitin like modifier activating enzyme 5) interacts with GABARAP proteins and mediates membrane localization of UBA5. *Autophagy*, 1-15.
INGELMO-TORRES, M., GONZALEZ-MORENO, E., KASSAN, A., HANZAL-BAYER, M., TEBAR, F., HERMS, A., GREWAL, T., HANCOCK, J. F., ENRICH, C., BOSCH, M., GROSS, S. P., PARTON, R. G. & POL, A. 2009. Hydrophobic and basic domains target proteins to lipid droplets. *Traffic,* 10**,** 1785-801.
KALVARI, I., TSOMPANIS, S., MULAKKAL, N. C., OSGOOD, R., JOHANSEN, T., NEZIS, I. P. & PROMPONAS, V. J. 2014. iLIR: A web resource for prediction of Atg8-family interacting proteins. *Autophagy,* 10**,** 913-25.
KARAGOZ, G. E., ACOSTA-ALVEAR, D. & WALTER, P. 2019. The Unfolded Protein Response: Detecting and Responding to Fluctuations in the Protein-Folding Capacity of the Endoplasmic Reticulum. *Cold Spring Harb Perspect Biol,* 11.
KASSAN, A., HERMS, A., FERNANDEZ-VIDAL, A., BOSCH, M., SCHIEBER, N. L., REDDY, B. J., FAJARDO, A., GELABERT-BALDRICH, M., TEBAR, F., ENRICH, C., GROSS, S. P., PARTON, R. G. & POL, A. 2013. Acyl-CoA synthetase 3 promotes lipid droplet biogenesis in ER microdomains. *J Cell Biol,* 203**,** 985-1001.
KAULICH, M. & DOWDY, S. F. 2015. Combining CRISPR/Cas9 and rAAV Templates for Efficient Gene Editing. *Nucleic Acid Ther,* 25**,** 287-96.
KELLEHER, D. J., KREIBICH, G. & GILMORE, R. 1992. Oligosaccharyltransferase activity is associated with a protein complex composed of ribophorins I and II and a 48 kd protein. *Cell,* 69**,** 55-65.
KIMURA, H., ARASAKI, K., OHSAKI, Y., FUJIMOTO, T., OHTOMO, T., YAMADA, J. & TAGAYA, M. 2018. Syntaxin 17 promotes lipid droplet formation by regulating the distribution of acyl-CoA synthetase 3. *J Lipid Res,* 59**,** 805-819.
KIRKIN, V. & ROGOV, V. V. 2019. A Diversity of Selective Autophagy Receptors Determines the Specificity of the Autophagy Pathway. *Mol Cell,* 76**,** 268-285.
KOMATSU, M., CHIBA, T., TATSUMI, K., IEMURA, S., TANIDA, I., OKAZAKI, N., UENO, T., KOMINAMI, E., NATSUME, T. & TANAKA, K. 2004. A novel protein-conjugating system for Ufm1, a ubiquitin-fold modifier. *EMBO J,* 23**,** 1977-86.
LE GUERROUE, F., ECK, F., JUNG, J., STARZETZ, T., MITTELBRONN, M., KAULICH, M. & BEHRENDS, C. 2017. Autophagosomal Content Profiling Reveals an LC3C-Dependent Piecemeal Mitophagy Pathway. *Mol Cell,* 68**,** 786-796 e6.
LEGESSE-MILLER, A., SAGIV, Y., PORAT, A. & ELAZAR, Z. 1998. Isolation and characterization of a novel low molecular weight protein involved in intra-Golgi traffic. *J Biol Chem,* 273**,** 3105-9.
LEIL, T. A., CHEN, Z. W., CHANG, C. S. & OLSEN, R. W. 2004. GABAA receptor-associated protein traffics GABAA receptors to the plasma membrane in neurons. *J Neurosci,* 24**,** 11429-38.
LEMAIRE, K., MOURA, R. F., GRANVIK, M., IGOILLO-ESTEVE, M., HOHMEIER, H. E., HENDRICKX, N., NEWGARD, C. B., WAELKENS, E., CNOP, M. & SCHUIT, F. 2011. Ubiquitin fold modifier 1 (UFM1) and its target UFBP1 protect pancreatic beta cells from ER stress-induced apoptosis. *PLoS One,* 6**,** e18517.
LIANG, J. H., LINGEMAN, E., LUONG, T., AHMED, S., NGUYEN, T., OLZMANN, J. & CORN, J. E. 2019. A genome-wide screen for ER autophagy highlights key roles of mitochondrial metabolism and ER-resident UFMylation. *bioRxiv*.
LIANG, J. R., LINGEMAN, E., AHMED, S. & CORN, J. E. 2018. Atlastins remodel the endoplasmic reticulum for selective autophagy. *J Cell Biol,* 217**,** 3354-3367.
LIU, J., WANG, Y., SONG, L., ZENG, L., YI, W., LIU, T., CHEN, H., WANG, M., JU, Z. & CONG, Y. S. 2017. A critical role of DDRGK1 in endoplasmic reticulum homoeostasis via regulation of IRE1alpha stability. *Nat Commun,* 8**,** 14186.
MARSHALL, R. S., LI, F., GEMPERLINE, D. C., BOOK, A. J. & VIERSTRA, R. D. 2015. Autophagic Degradation of the 26S Proteasome Is Mediated by the Dual ATG8/Ubiquitin Receptor RPN10 in Arabidopsis. *Mol Cell,* 58**,** 1053-66.

MARSHALL, R. S. & VIERSTRA, R. D. 2019. Dynamic Regulation of the 26S Proteasome: From Synthesis to Degradation. *Front Mol Biosci,* 6**,** 40.
MATIC, I., SCHIMMEL, J., HENDRIKS, I. A., VAN SANTEN, M. A., VAN DE RIJKE, F., VAN DAM, H., GNAD, F., MANN, M. & VERTEGAAL, A. C. 2010. Site-specific identification of SUMO-2 targets in cells reveals an inverted SUMOylation motif and a hydrophobic cluster SUMOylation motif. *Mol Cell,* 39**,** 641-52.
MIZUSHIMA, N., YOSHIMORI, T. & OHSUMI, Y. 2011. The role of Atg proteins in autophagosome formation. *Annu Rev Cell Dev Biol,* 27**,** 107-32.
MULLER, J. M., SHORTER, J., NEWMAN, R., DEINHARDT, K., SAGIV, Y., ELAZAR, Z., WARREN, G. & SHIMA, D. T. 2002. Sequential SNARE disassembly and GATE-16-GOS-28 complex assembly mediated by distinct NSF activities drives Golgi membrane fusion. *J Cell Biol,* 157**,** 1161-73.
NGUYEN, T. N., PADMAN, B. S., USHER, J., OORSCHOT, V., RAMM, G. & LAZAROU, M. 2016. Atg8 family LC3/GABARAP proteins are crucial for autophagosome-lysosome fusion but not autophagosome formation during PINK1/Parkin mitophagy and starvation. *J Cell Biol,* 215**,** 857-874.
NODA, N. N., KUMETA, H., NAKATOGAWA, H., SATOO, K., ADACHI, W., ISHII, J., FUJIOKA, Y., OHSUMI, Y. & INAGAKI, F. 2008. Structural basis of target recognition by Atg8/LC3 during selective autophagy. *Genes Cells,* 13**,** 1211-8.
PANKIV, S., CLAUSEN, T. H., LAMARK, T., BRECH, A., BRUUN, J. A., OUTZEN, H., OVERVATN, A., BJORKOY, G. & JOHANSEN, T. 2007. p62/SQSTM1 binds directly to Atg8/LC3 to facilitate degradation of ubiquitinated protein aggregates by autophagy. *J Biol Chem,* 282**,** 24131-45.
POPOVIC, D., AKUTSU, M., NOVAK, I., HARPER, J. W., BEHRENDS, C. & DIKIC, I. 2012. Rab GTPase-activating proteins in autophagy: regulation of endocytic and autophagy pathways by direct binding to human ATG8 modifiers. *Mol Cell Biol,* 32**,** 1733-44.
POPPELREUTHER, M., RUDOLPH, B., DU, C., GROSSMANN, R., BECKER, M., THIELE, C., EHEHALT, R. & FULLEKRUG, J. 2012. The N-terminal region of acyl-CoA synthetase 3 is essential for both the localization on lipid droplets and the function in fatty acid uptake. *J Lipid Res,* 53**,** 888-900.
ROGOV, V., DOTSCH, V., JOHANSEN, T. & KIRKIN, V. 2014. Interactions between autophagy receptors and ubiquitin-like proteins form the molecular basis for selective autophagy. *Mol Cell,* 53**,** 167-78.
ROLLAND, T., TASAN, M., CHARLOTEAUX, B., PEVZNER, S. J., ZHONG, Q., SAHNI, N., YI, S., LEMMENS, I., FONTANILLO, C., MOSCA, R., KAMBUROV, A., GHIASSIAN, S. D., YANG, X., GHAMSARI, L., BALCHA, D., BEGG, B. E., BRAUN, P., BREHME, M., BROLY, M. P., CARVUNIS, A. R., CONVERY-ZUPAN, D., COROMINAS, R., COULOMBE-HUNTINGTON, J., DANN, E., DREZE, M., DRICOT, A., FAN, C., FRANZOSA, E., GEBREAB, F., GUTIERREZ, B. J., HARDY, M. F., JIN, M., KANG, S., KIROS, R., LIN, G. N., LUCK, K., MACWILLIAMS, A., MENCHE, J., MURRAY, R. R., PALAGI, A., POULIN, M. M., RAMBOUT, X., RASLA, J., REICHERT, P., ROMERO, V., RUYSSINCK, E., SAHALIE, J. M., SCHOLZ, A., SHAH, A. A., SHARMA, A., SHEN, Y., SPIROHN, K., TAM, S., TEJEDA, A. O., TRIGG, S. A., TWIZERE, J. C., VEGA, K., WALSH, J., CUSICK, M. E., XIA, Y., BARABASI, A. L., IAKOUCHEVA, L. M., ALOY, P., DE LAS RIVAS, J., TAVERNIER, J., CALDERWOOD, M. A., HILL, D. E., HAO, T., ROTH, F. P. & VIDAL, M. 2014. A proteome-scale map of the human interactome network. *Cell,* 159**,** 1212-1226.
SCHAAF, M. B., KEULERS, T. G., VOOIJS, M. A. & ROUSCHOP, K. M. 2016. LC3/GABARAP family proteins: autophagy-(un)related functions. *FASEB J,* 30**,** 3961-3978.
SHPILKA, T., WEIDBERG, H., PIETROKOVSKI, S. & ELAZAR, Z. 2011. Atg8: an autophagy-related ubiquitin-like protein family. *Genome Biol,* 12**,** 226.
SLOBODKIN, M. R. & ELAZAR, Z. 2013. The Atg8 family: multifunctional ubiquitin-like key regulators of autophagy. *Essays Biochem,* 55**,** 51-64.
SOUPENE, E. & KUYPERS, F. A. 2008. Mammalian long-chain acyl-CoA synthetases. *Exp Biol Med (Maywood),* 233**,** 507-21.

STADEL, D., MILLARTE, V., TILLMANN, K. D., HUBER, J., TAMIN-YECHESKEL, B. C., AKUTSU, M., DEMISHTEIN, A., BEN-ZEEV, B., ANIKSTER, Y., PEREZ, F., DOTSCH, V., ELAZAR, Z., ROGOV, V., FARHAN, H. & BEHRENDS, C. 2015. TECPR2 Cooperates with LC3C to Regulate COPII-Dependent ER Export. *Mol Cell,* 60**,** 89-104.
STOLZ, A., ERNST, A. & DIKIC, I. 2014. Cargo recognition and trafficking in selective autophagy. *Nat Cell Biol,* 16**,** 495-501.
STOLZ, A., PUTYRSKI, M., KUTLE, I., HUBER, J., WANG, C., MAJOR, V., SIDHU, S. S., YOULE, R. J., ROGOV, V. V., DOTSCH, V., ERNST, A. & DIKIC, I. 2017. Fluorescence-based ATG8 sensors monitor localization and function of LC3/GABARAP proteins. *EMBO J,* 36**,** 549-564.
TATSUMI, K., SOU, Y. S., TADA, N., NAKAMURA, E., IEMURA, S., NATSUME, T., KANG, S. H., CHUNG, C. H., KASAHARA, M., KOMINAMI, E., YAMAMOTO, M., TANAKA, K. & KOMATSU, M. 2010. A novel type of E3 ligase for the Ufm1 conjugation system. *J Biol Chem,* 285**,** 5417-27.
TATSUMI, K., YAMAMOTO-MUKAI, H., SHIMIZU, R., WAGURI, S., SOU, Y. S., SAKAMOTO, A., TAYA, C., SHITARA, H., HARA, T., CHUNG, C. H., TANAKA, K., YAMAMOTO, M. & KOMATSU, M. 2011. The Ufm1-activating enzyme Uba5 is indispensable for erythroid differentiation in mice. *Nat Commun,* 2**,** 181.
WALCZAK, C. P., LETO, D. E., ZHANG, L., RIEPE, C., MULLER, R. Y., DAROSA, P. A., INGOLIA, N. T., ELIAS, J. E. & KOPITO, R. R. 2019. Ribosomal protein RPL26 is the principal target of UFMylation. *Proc Natl Acad Sci U S A,* 116**,** 1299-1308.
WANG, H., BEDFORD, F. K., BRANDON, N. J., MOSS, S. J. & OLSEN, R. W. 1999. GABA(A)-receptor-associated protein links GABA(A) receptors and the cytoskeleton. *Nature,* 397**,** 69-72.
WEIDBERG, H., SHPILKA, T., SHVETS, E., ABADA, A., SHIMRON, F. & ELAZAR, Z. 2011. LC3 and GATE-16 N termini mediate membrane fusion processes required for autophagosome biogenesis. *Dev Cell,* 20**,** 444-54.
WU, J., LEI, G., MEI, M., TANG, Y. & LI, H. 2010. A novel C53/LZAP-interacting protein regulates stability of C53/LZAP and DDRGK domain-containing Protein 1 (DDRGK1) and modulates NF-kappaB signaling. *J Biol Chem,* 285**,** 15126-36.
XIE, Z., NAIR, U. & KLIONSKY, D. J. 2008. Atg8 controls phagophore expansion during autophagosome formation. *Mol Biol Cell,* 19**,** 3290-8.
YOO, H. M., KANG, S. H., KIM, J. Y., LEE, J. E., SEONG, M. W., LEE, S. W., KA, S. H., SOU, Y. S., KOMATSU, M., TANAKA, K., LEE, S. T., NOH, D. Y., BAEK, S. H., JEON, Y. J. & CHUNG, C. H. 2014. Modification of ASC1 by UFM1 is crucial for ERalpha transactivation and breast cancer development. *Mol Cell,* 56**,** 261-274.
ZHANG, M., ZHU, X., ZHANG, Y., CAI, Y., CHEN, J., SIVAPRAKASAM, S., GURAV, A., PI, W., MAKALA, L., WU, J., PACE, B., TUAN-LO, D., GANAPATHY, V., SINGH, N. & LI, H. 2015. RCAD/Ufl1, a Ufm1 E3 ligase, is essential for hematopoietic stem cell function and murine hematopoiesis. *Cell Death Differ,* 22**,** 1922-34.
ZHANG, Y., ZHANG, M., WU, J., LEI, G. & LI, H. 2012. Transcriptional regulation of the Ufm1 conjugation system in response to disturbance of the endoplasmic reticulum homeostasis and inhibition of vesicle trafficking. *PLoS One,* 7**,** e48587.
ZHU, H., BHATT, B., SIVAPRAKASAM, S., CAI, Y., LIU, S., KODEBOYINA, S. K., PATEL, N., SAVAGE, N. M., SHARMA, A., KAUFMAN, R. J., LI, H. & SINGH, N. 2019. Ufbp1 promotes plasma cell development and ER expansion by modulating distinct branches of UPR. *Nat Commun,* 10**,** 1084.

Figures

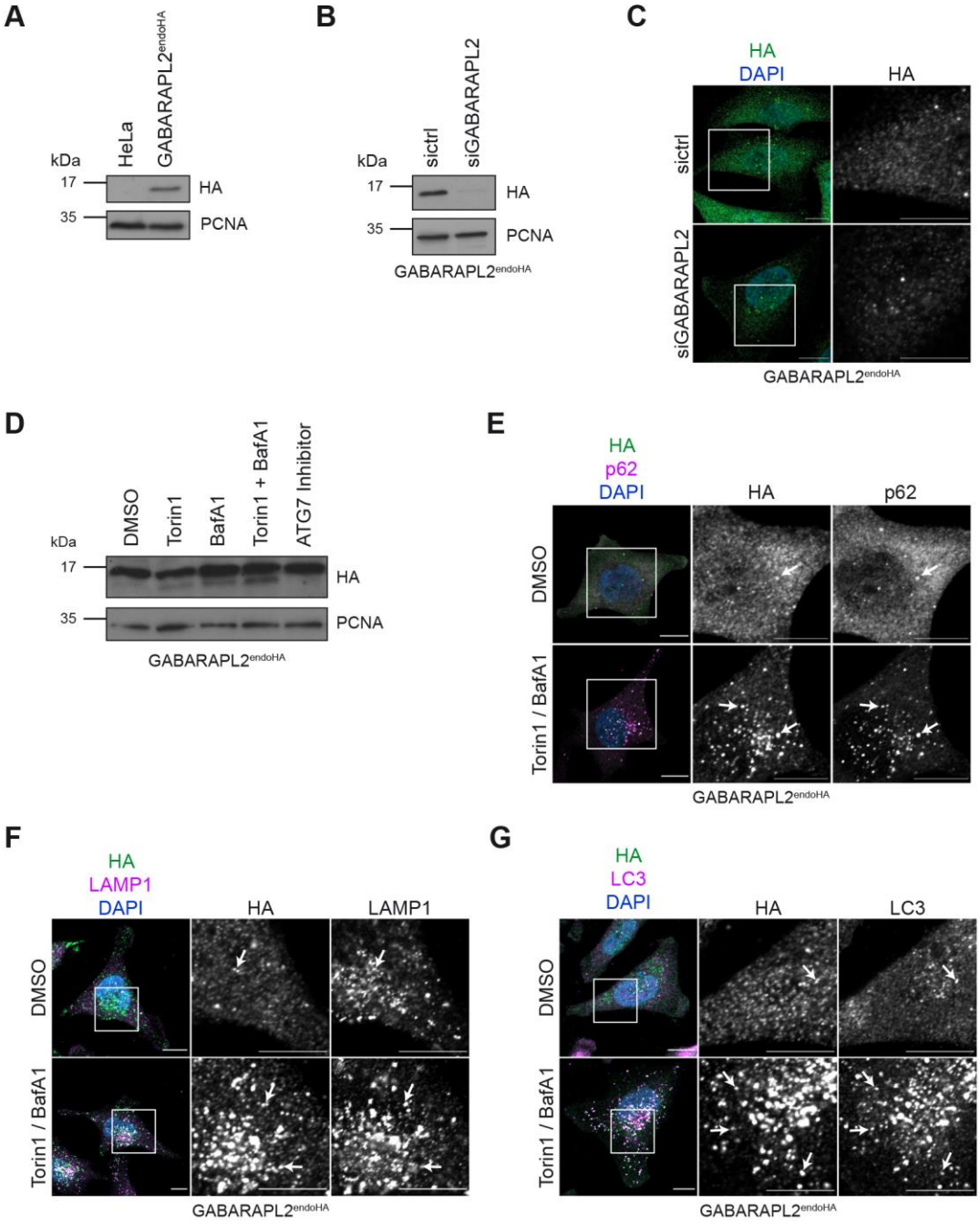

Fig. 1. Establishment of cells carrying endogenously HA-tagged LC3s and GABARAPs. (A) GABARAPL2^{endoHA} and parental HeLa cell lysates were analyzed by immunoblotting using anti-HA and -PCNA antibodies. The latter was used as loading control. (B,C) GABARAPL2^{endoHA} cells were reversely transfected for 72 hrs with non-targeting (sictrl) or GABARAPL2 siRNA followed by lysis and immunoblot analysis (B) or fixation and immunolabeling (C) using an anti-HA antibody. Scale bar: 10 µm. (D) GABARAPL2^{endoHA} cells were treated as indicated and subjected to lysis and immunoblotting. (E-G) GABARAPL2^{endoHA} cells treated with indicated inhibitors were immunolabeled with anti-p62 (E), anti-LAMP1 (F) or anti-LC3 (G) antibodies. Scale bar: 10 µm. Arrowheads indicate colocalization events.

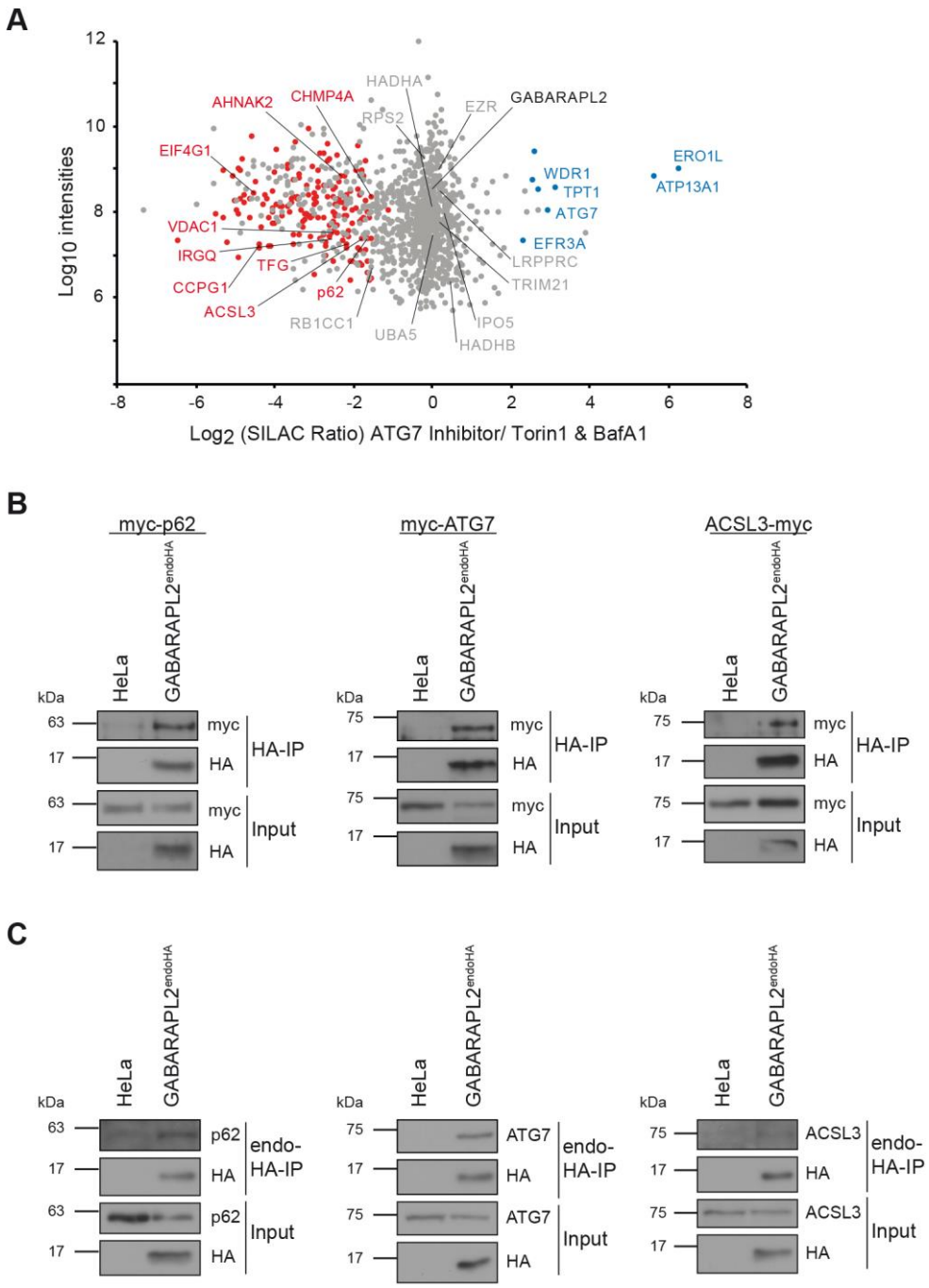

Fig. 2. Endogenous GABARAPL2 interactome. (A) Scatterplot represents interaction proteomics of SILAC labeled GABARAPL2^{endoHA} cells differentially treated with Torin1 and BafA1 (light) or ATG7 inhibitor (heavy). Significantly enriched proteins upon Torin1 and BafA1 combination treatment or ATG7 inhibition are highlighted in red and blue, respectively. Proteins in grey are unchanged. (B,C) Immunoblot analysis of anti-HA immunoprecipitates from lysates derived from parental HeLa and GABARAPL2^{endoHA} cells which were either transiently transfected for 48 hrs with myc-tagged ATG7, p62 or ACSL3 (B) or left untreated (C).

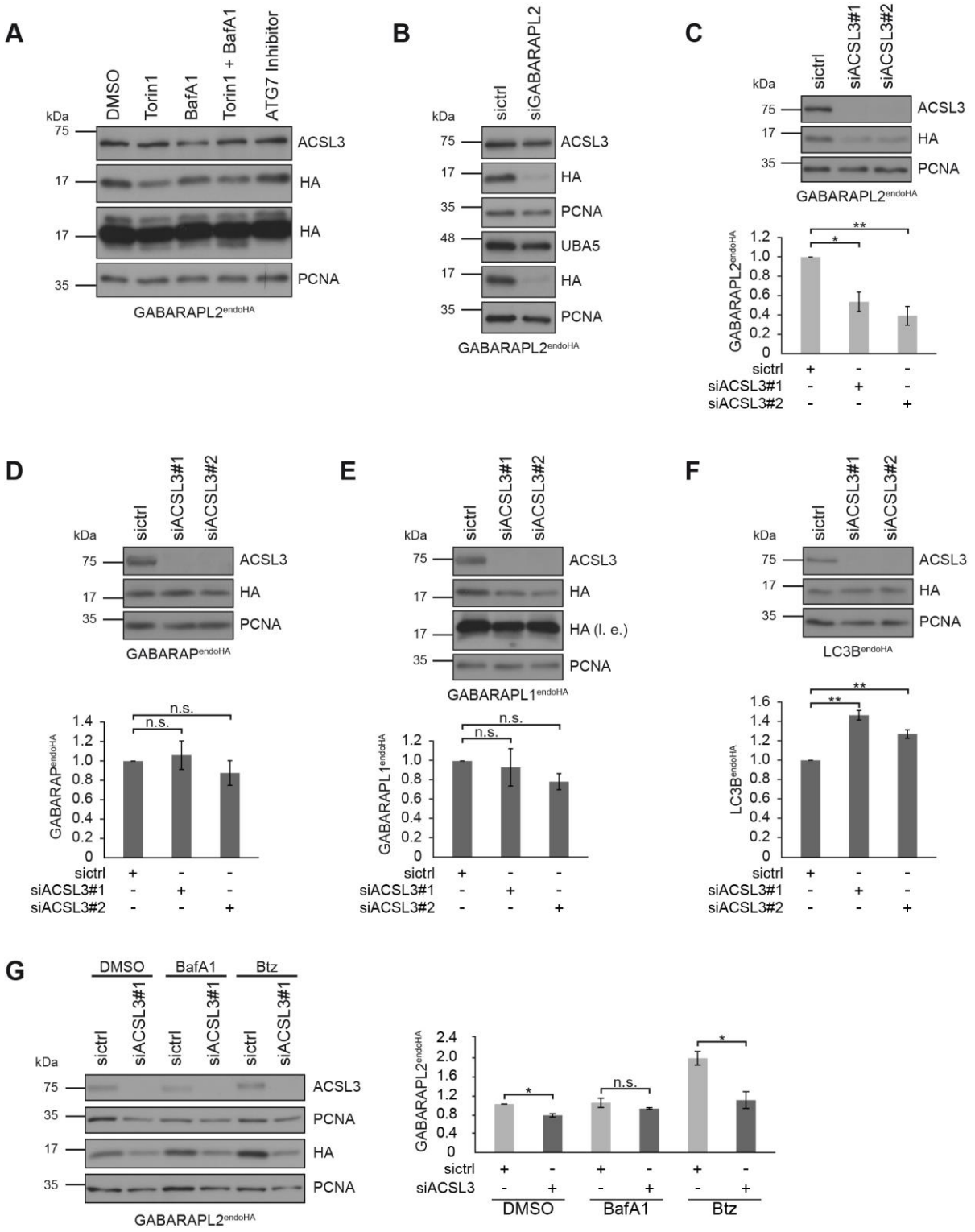

Fig. 3. Stabilization of GABARAPL2 through ACSL3. (A) GABARAPL2^{endoHA} cells were treated as indicated and subjected to lysis and analyzed with immunoblotting and anti-ACSL3 antibody. (B) Reversely transfected GABARAPL2^{endoHA} cells with non-targeting (sictrl) or

GABARAPL2 siRNA were lysed followed by immunoblotting and analysis with indicated antibodies. **(**C-F) GABARAPL2^{endoHA} (C), GABARAP^{endoHA} (D), GABARAPL1^{endoHA} (E) and LC3B^{endoHA} (F) cells were reversely transfected with two different ACSL3 siRNAs. Lysates were analyzed by immunoblotting with indicated antibodies. Data represent mean ±SEM. Statistical analysis (n = 4) of the HA/PCNA ratio normalized to sictrl was performed using Student's t-test (*p<0.05, **p<0.01). (G) GABARAPL2^{endoHA} cells reversely transfected with siRNAs targeting ACSL3 for 72 hrs were treated with BafA1 or Btz and analyzed by immunoblotting. Data represents mean ±SEM. Statistical analysis (n = 3) of the HA/PCNA ratio normalized to sictrl-DMSO, was performed using Student's t-test (*p<0.05).

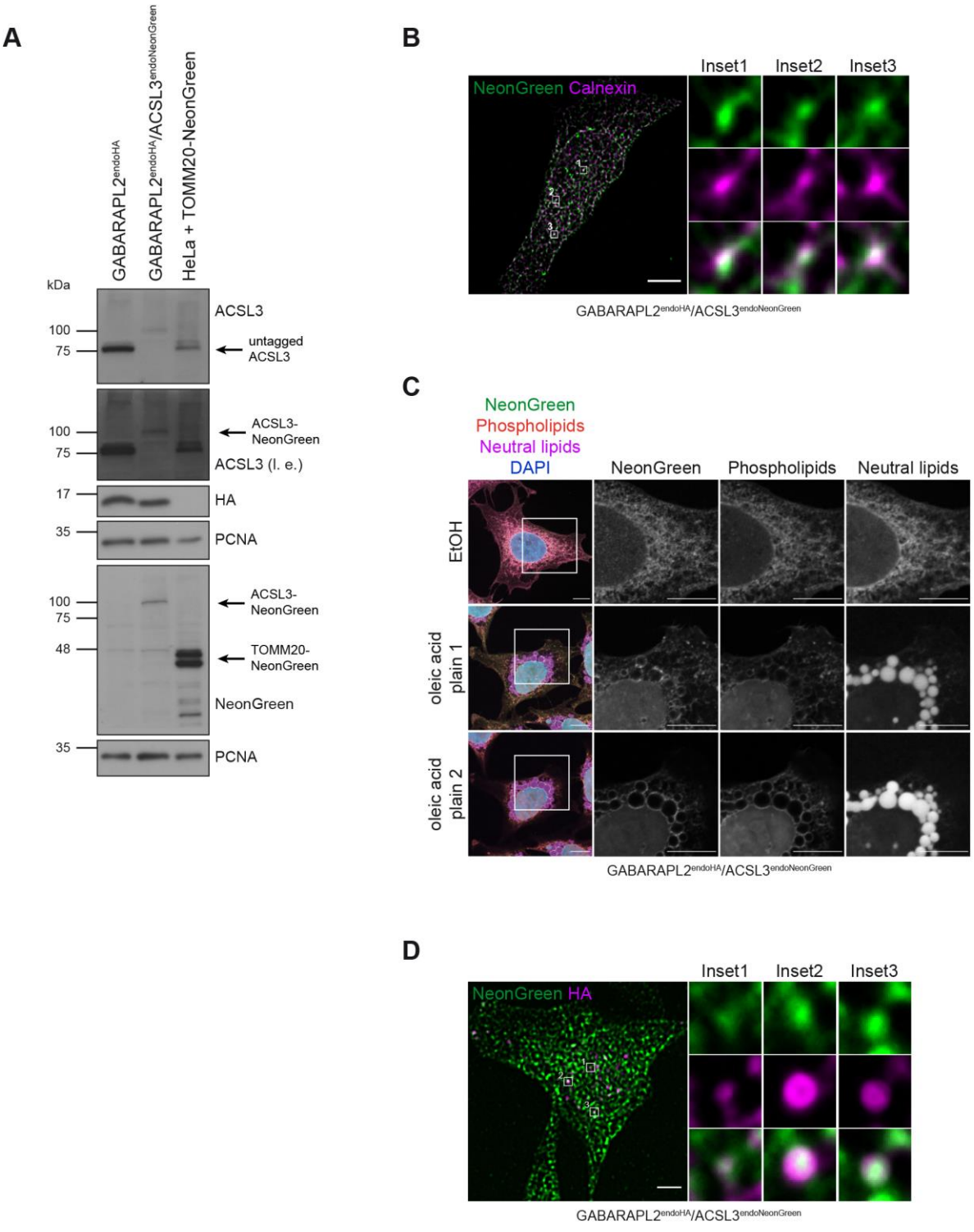

Fig. 4. Colocalization of GABARAPL2 and ACSL3 at the ER. (A) GABARAPL2^{endoHA} and GABARAPL2^{endoHA}/ACSL3^{endoNeonGreen} cells as well as parental HeLa cells transiently transfected with TOMM20-NeonGreen were lysed and analyzed by immunoblotting with indicated antibodies. (B), Representative SRRF image of

GABARAPL2^{endoHA}/ACSL3^{endoNeonGreen} cells immunolabeled with anti-Calnexin. Magnified view of colocalization events of ACSL3^{endoNeonGreen} and the ER marker Calnexin are shown in insets. Scale bars: 5 µm. (C) GABARAPL2^{endoHA}/ACSL3^{endoNeonGreen} cells were treated with oleic acid or EtOH (control) for 24 hrs followed by fixation and labeling of phospholipids and neutral lipids with HCS LipidTox lipid stains. Scale bar: 10 µm. Two confocal planes are shown for oleic acid treatment. (D), Representative SRRF image of GABARAPL2^{endoHA}/ACSL3^{endoNeonGreen} cells after immunolabeling with anti-HA. Insets show magnified view of colocalization events. Scale bars: 5 µm.

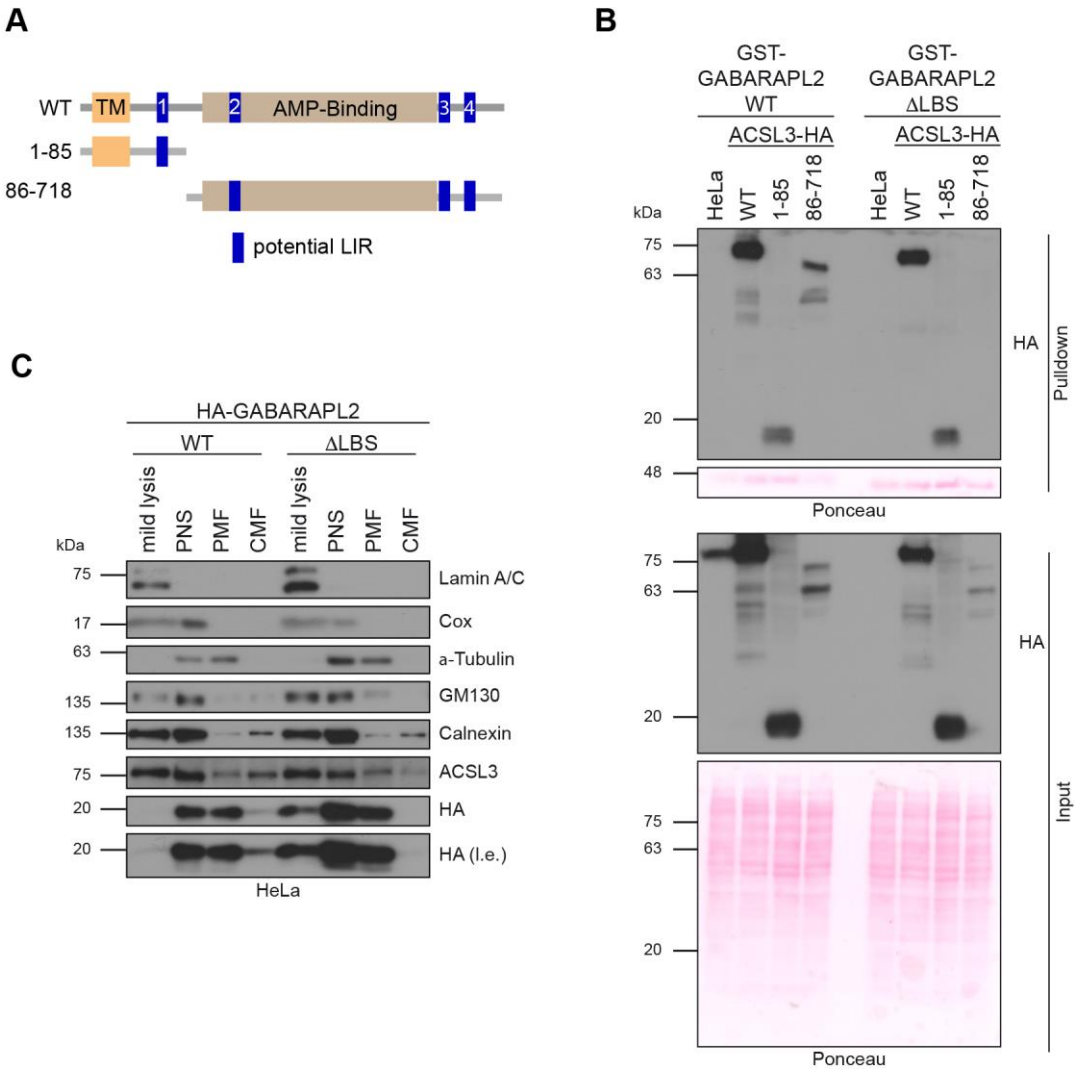

Fig. 5. LDS of GABARAPL2 mediate ACSL3 binding and ER recruitment. (A) Scheme of wild-type (WT) ACSL3 and fragments with known domains and potential LIRs. (B) Pulldown assays using GST-tagged WT or ΔLBS GABARAPL2 protein incubated with lysates from HeLa cells expressing WT or fragmented ACSL3 were analyzed by immunoblotting and Ponceau staining. (D) Subcellular fractionation of HeLa cells stably expressing WT or ΔLBS GABARAPL2 followed by immunoblot analysis with indicated antibodies. PNS, post nuclear fraction; PMF, post mitochondrial fraction; CMF, crude microsomal fraction.

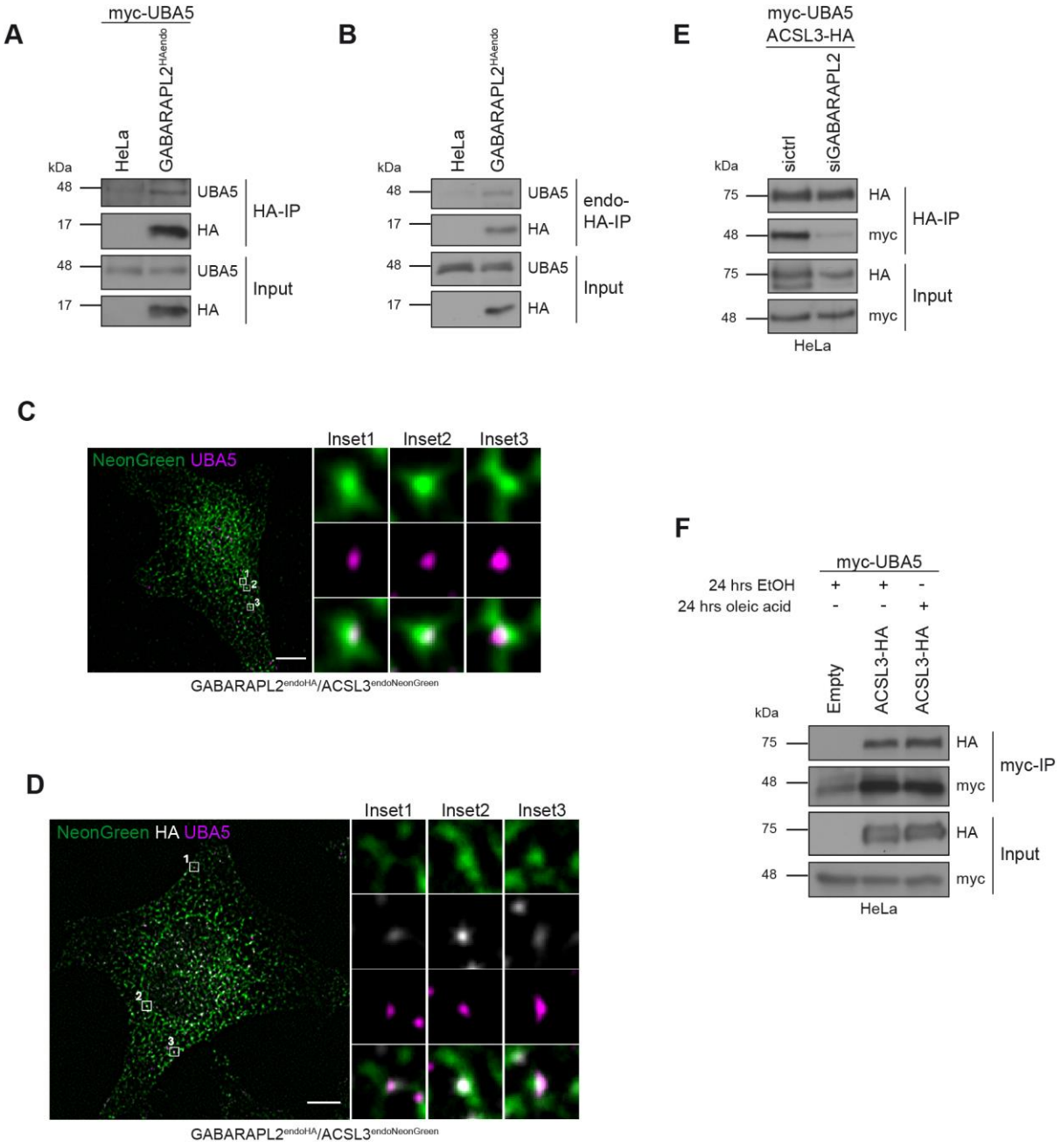

Fig. 6. UBA5 binds to and colocalizes with ACSL3 and GABARAPL2. (A, B) Immunoblot analysis of anti-HA immunoprecipitates from lysates derived from parental HeLa and GABARAPL2^{endoHA} cells either transiently transfected for 48 hrs with myc-UBA5 (A) or left untreated (B) and analyzed with indicated antibodies. (C) Representative SRRF image of GABARAPL2^{endoHA}/ACSL3^{endoNeonGreen} cells immunolabeled with anti-UBA5. Colocalization events of ACSL3^{endoNeonGreen} and UBA5 are shown enlarged in insets. Scale bars: 5 µm. (D) Representative SRRF image of GABARAPL2^{endoHA}/ACSL3^{endoNeonGreen} cells labeled with anti-

HA and -UBA5. Colocalization events of ACSL3^{endoNeonGreen}, GABARAPL2^{endoHA} and UBA5 are shown in magnified insets. Scale bars: 5 µm. (E) Stable expressing ACSL3-HA cells were reverse transfected with sictrl or siGABARAPL2 for 72 hrs and transiently transfected with myc-UBA5 for 48 hrs followed by lysis, anti-HA immunoprecipitation and immunoblot analysis. (F) Parental HeLa and GABARAPL2^{endoHA} cells transfected with myc-UBA5 were treated with oleic acid or EtOH for 24 hrs prior to lysis, anti-myc immunoprecipitation and immunoblotting.

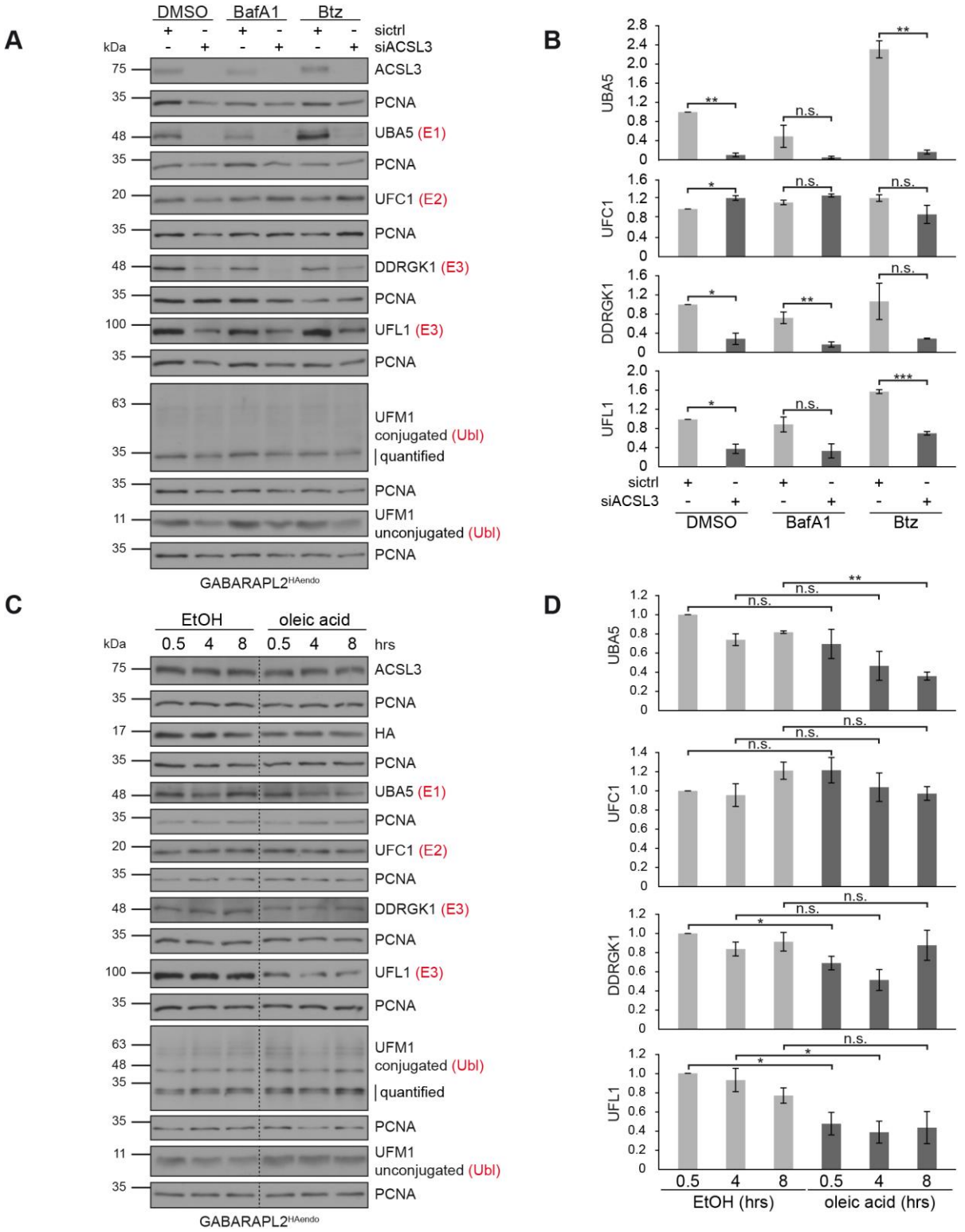

Fig. 7. ACSL3 and LD biogenesis regulate the ufmylation pathway. (A) GABARAPL2^{endoHA} cells were transfected with ACSL3 siRNAs and treated with Btz or BafA1 followed by lysis and immunoblot analysis using indicated antibodies. (B) Quantitative analysis of A. Data

represents mean ±SEM. Statistical analysis (n = 3) of the indicated protein/PCNA ratio normalized to sictrl-DMSO was performed using Student's t-test (*p<0.05, **p<0.01, ***p<0.001). (C) GABARAPL2^{endoHA} cells were treated with oleic acid or EtOH for 0.5, 4 or 8 hrs prior to lysis and immunoblotting with indicated antibodies. (D) Quantitative analysis of C. Data represents mean ±SEM. Statistical analysis (n = 3) of the indicated protein/PCNA ratio normalized to 0.5 hrs EtOH was performed using Student's t-test (*p<0.05, **p<0.01).

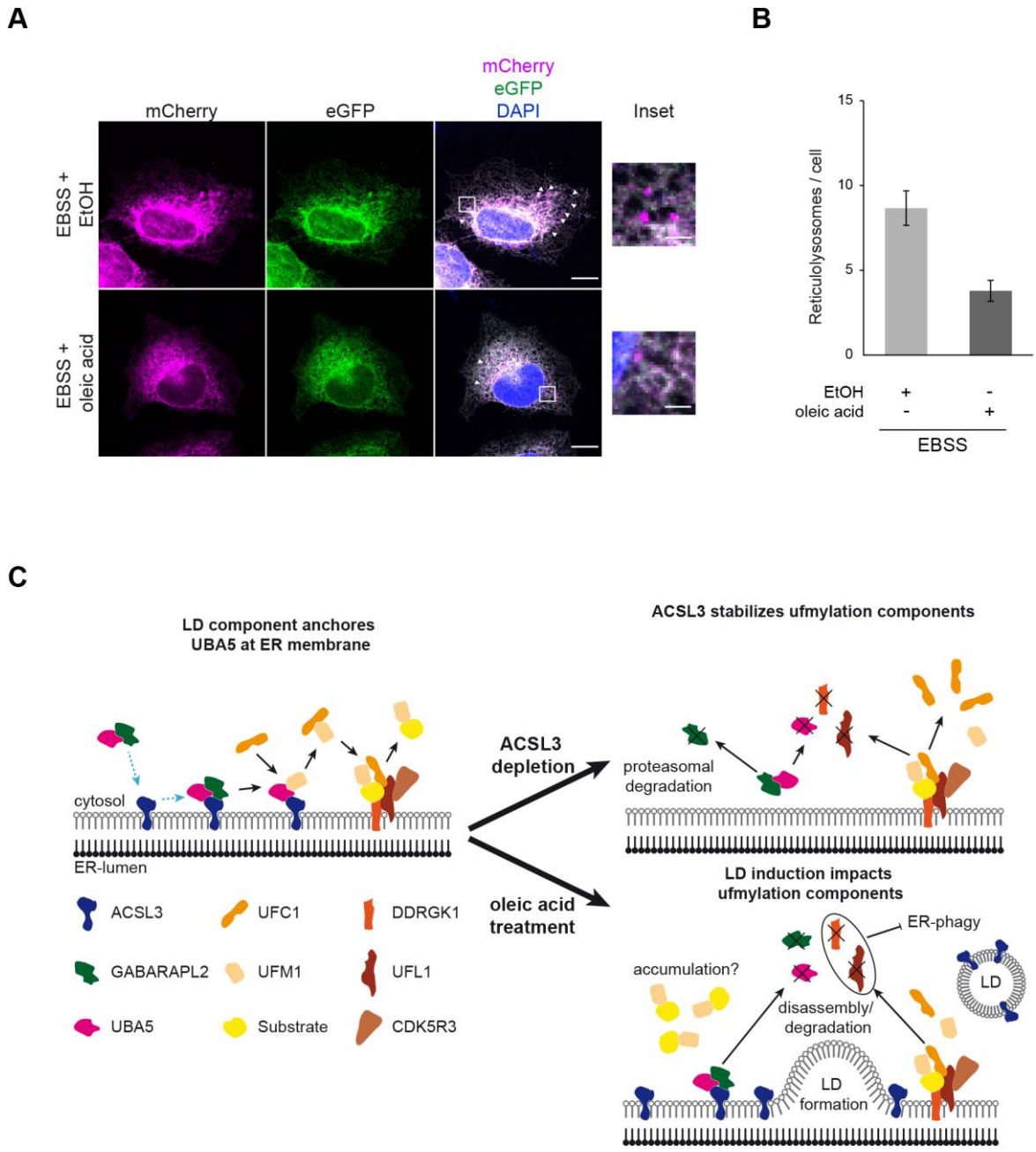

Fig. 8. Oleic acid inhibits ER-phagy. (A) HeLa cells were transiently transfected with mCherry-eGFP-RAMP4 and starved with EBSS for 8 hrs in combination with either EtOH or oleic acid. Red-only puncta were defined as reticulolysosomes. Scale bar: 10 μm. Inset scale bar: 2 μm. Arrowheads indicate reticulolysosomes. (B) Quantitative analysis of A. Data represents mean ±SEM. Statistical analysis (n = 3) was performed using Student's t-test (*p<0.05). (C) Working model of ACSL3's role in the ufmylation pathway. UBA5 is recruited to ACSL3 by GABARAPL2. Upon loss of ACSL3 or induction of LD biogenesis ufmylation components are downregulated and dynamics of UFM1 conjugation are altered. Dotted blue arrows indicate ER-recruitment, black arrows indicate ufmylation cascade.

A

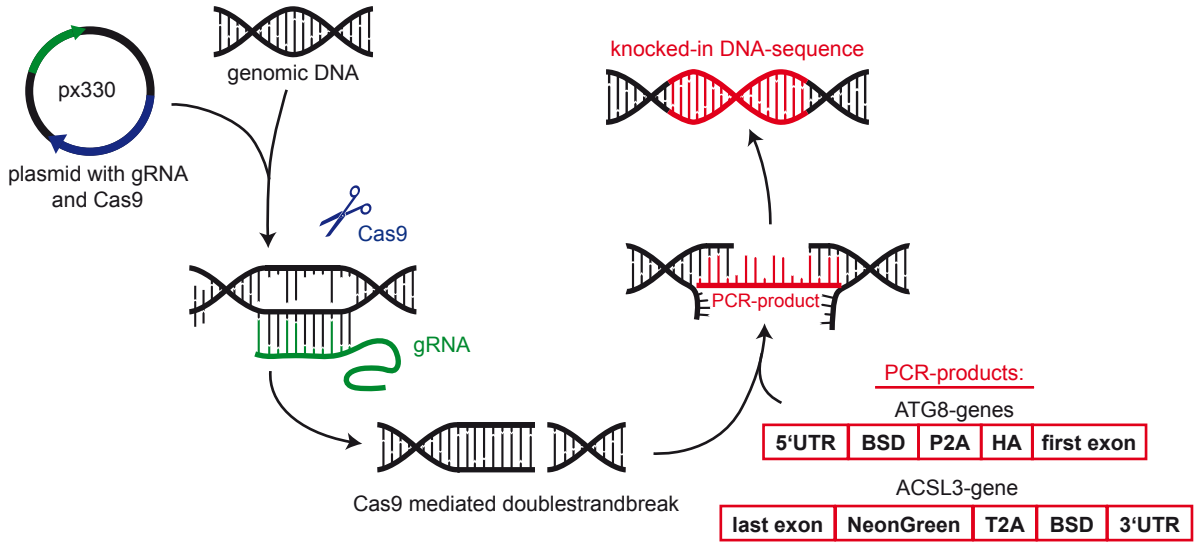

B

GABARAP^{endoHA}: TTCGTGGATCGCTCCGCTGAATCCGCCCGCGCGTCGCCGCCGTCGTCGCCGCCCCCCGTCCCGGCCCCCCTGGGTTCCCTCAGCCCAGCCCTGTCCA
GCCCGGTTCCGGGGAGGATGAAGCCGGCC**AAGCCTTTGTCTCAAGAAGAATCCACCCTCATTGAAAGAGCAACGGCTACAATCAACAGCATCCCCATCTCTGAAGACTA**
CAGCGTCGCCAGCGCAGCTCTCTCTAGCGACGGCCGCATCTTCACTGGTGTCAATGTATATCATTTTACTGGGGGACCTTGTGCAGAACTCGTGGTGCTGGGCACTGCT
GCTGCTGCGGCAGCTGGCAACCTGACTTGTATCGTCGCGATCGGAAATGAGAACAGGGGCATCTTGAGCCCCTGCGGACGGTGCCGACAGGTGCTTCTCGATCTGCATC
CTGGGATCAAAGCCATAGTGAAGGACAGTGATGGACAGCCGACGGCAGTTGGGATTCGTGAATTGCTGCCCTCTGGTTATGT

GABARAPL1^{endoHA}: TGCACACTCGGCCCAGCGCTGTTGCCCCCGGAGCGGACGTTTCTGCAGCTATTCTGAGCACACCTTGACGTCGGCTGAGGGAGCGGGACAGGGTC
AGCGGCGAAGGAGGCAGGCCCCGCGCGGGGATCTCGGAAGCGCTGCGGTGCATCATG**AAGCCGGCCAAGCCTTTGTCTCAAGAAGAATCCACCCTCATTGAAAGAGCAA**
CGGCTACAATCAACAGCATCCCCATCTCTGAAGACTACAGCGTCGCCAGCGCAGCTCTCTCTAGCGACGGCCGCATCTTCACTGGTGTCAATGTATATCATTTTACTGG
GGGACCTTGTGCAGAACTCGTGGTGCTGGGCACTGCTGCTGCTGCGGCAGCTGGCAACCTGACTTGTATCGTCGCGATCGGAAATGAGAACAGGGGCATCTTGAGCCCC
TGCGGACGGTGCCGACAGGTGCTTCTCGATCTGCATCCTGGGATCAAAGCCATAGTGAAGGACAGTGATGGACAGCCGACGGCAGTTGGGATTCGTGAATTGCTGCCC

GABARAPL2^{endoHA}: GCCCCTTTACGTGCGGCCCCGCCCCTTGGCGTGGCGCCCTGACAAATGGCGCCGGAAGCCCCGCCCCCGGCCGGTTGCTAGGCTCCGACAGCCGG
AAGTCCCGCCTGCCGTGTAGTCGCCGCCGTCGCTGCCGCTGCCGCTGCCGCCGTCGTTGTTGTTGTGCTCGGTGCGCTGAGCTCCGCGGCTCCGCGAGCCGGTTCCGTC
CCCTTCCCGCCGCGGCCATG**AAGCCGGCCAAGCCTTTGTCTCAAGAAGAATCCACCCTCATTGAAAGAGCAACGGCTACAATCAACAGCATCCCCATCTCTGAAGACTA**
CAGCGTCGCCAGCGCAGCTCTCTCTAGCGACGGCCGCATCTTCACTGGTGTCAATGTATATCATTTTACTGGGGGACCTTGTGCAGAACTCGTGGTGCTGGGCACTGCT
GCTGCTGCGGCAGCTGGCAACCTGACTTGTATCGTCGCGATCGGAAATGAGAACAGGGGCATCTTGAGCCCCTGCGGACGGTGCCGACAGGTGCTTCTCGATCTGCATC
CTGGGATCAAAGCCATAGTGAAGGACAGTGATGGACAGCCGACGGCAGTTGGGATTCGTGAATTGCTGCCCTCTGGTTATGTGTGGGAGGGC

LC3B^{endoHA}: CTGCGTGCCGCTGCTGGGTTCCGCCACGCCCGTCATGGCGGCGGCCCCGGCCGGCTCTGGCCCCGCCCCTCGGTGACGCGTCGCGAGTCACCTGACCAGG
CTGCGGGCTGAGGAGATACAAGGGAAGTGGCTATCGCCAGAGTCGGATTCGCCGCCGCAGCAGCCGCCGCCCCCGGGAGCCGCCGGGACCCTCGCGTCGTCGCCGCCGC
CGCCGCCCAGATCCCTGCACCATG**CCGGCCAAGCCTTTGTCTCAAGAAGAATCCACCCTCATTGAAAGAGCAACGGCTACAATCAACAGCATCCCCATCTCTGAAGACT**
ACAGCGTCGCCAGCGCAGCTCTCTCTAGCGACGGCCGCATCTTCACTGGTGTCAATGTATATCATTTTACTGGGGGACCTTGTGCAGAACTCGTGGTGCTGGGCACTGC
TGCTGCTGCGGCAGCTGGCAACCTGACTTGTATCGTCGCGATCGGAAATGAGAACAGGGGCATCTTGAGCCCCTGCGGACGGTGCCGACAGGTGCTTCTCGATCTGCAT
CCTGGGATCAAAGCCATAGTGAAGGACAGTGATGGACAGCCGACGGCAGTTGGGATTCGTGAATTGCTGCCCTCTGGTTATGTGTGGGAGGGC

C

ACSL3^{endoNeonGreen}: TATTTTTTTTTAATCATCTTAGCAAGTCTGGAAAAGTTTGAAATTCCAGTAAAAATTCGTTTGAGTCATGAACCGTGGACCCCTGAAACTGGTCT
GGTGACAGATGCCTTCAAGCTGAAACGCAAAGAGCTTAAAACACATTACCAGGCGGACATTGAGCGAATGTATGGAAGAAAA**GCTGGCGGCATGGTGAGCAAGGGCGAG**
GAGGATAACATGGCCTCTCTCCCAGCGACACATGAGTTACACATCTTTGGCTCCATCAACGGTGTGGACTTTGACATGGTGGGTCAGGGCACCGGCAATCCAAATGATG
GTTATGAGGAGTTAAACCTGAAGTCCACCAAGGGTGACCTCCAGTTCTCCCCCTGGATTCTGGTCCCTCATATCGGGTATGGCTTCCATCAGTACCTGCCCTACCCTGA
CGGGATGTCGCCTTTCCAGGCCGCCATGGTAGATGGCTCCGGATACCAAGTCCATCGCACAATGCAGTTTGAAGATGGTGCCT

Figure S1

Fig. S1. Endogenous epitope tagging of hATG8 and ACSL3 genes. (A) Experimental CRISPR/Cas9 workflow. (B,C) Sequence data from PCR products of the tagged GABARAP$_{endoHA}$, GABARAPL1$_{endoHA}$, GABARAPL2$_{endoHA}$, LC3B$_{endoHA}$ cell lines (B) and the GABARAPL2$_{endoHA}$/ACSL3$_{endoNeonGreen}$ cell line (C). Introduced CRISPR sequences are indicated in bold.

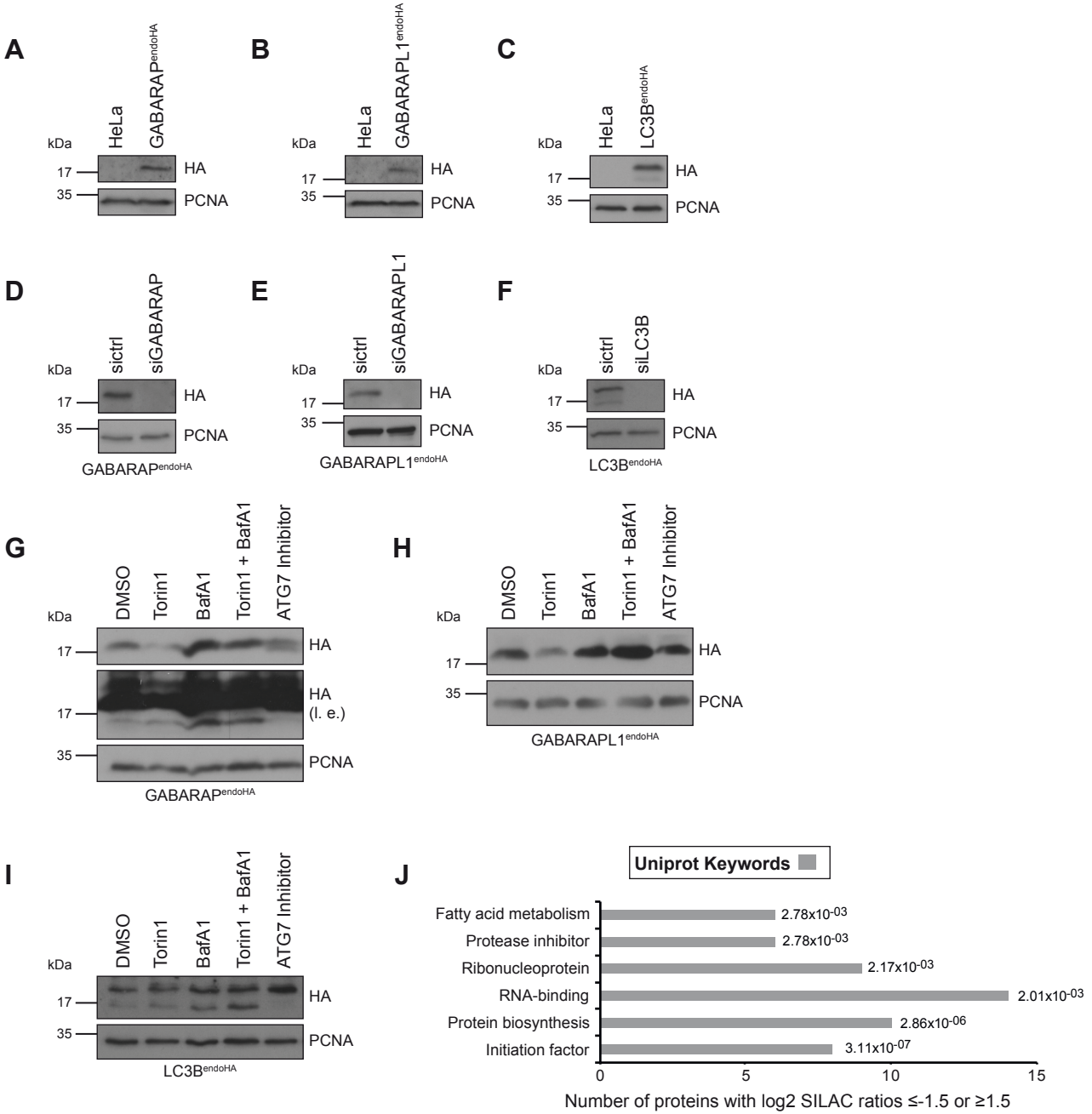

Figure S2

Fig. S2. Validation of endogenously HA-tagged hATG8 proteins. (A-C) GABARAP$_{endoHA}$ (A) GABARAPL1$_{endoHA}$ (B) LC3B$_{endoHA}$ (C) and parental HeLa (A-C) cells were lysed followed by immunoblotting and analysis with indicated antibodies. (D-F) GABARAP$_{endoHA}$ (D), GABARAPL1$_{endoHA}$ (E), LC3B$_{endoHA}$ (F) cell lines were reversely transfected with indicated siRNAs prior to immunoblot analysis. (G-I) GABARAP$_{endoHA}$ (G), GABARAPL1$_{endoHA}$ (H), LC3B$_{endoHA}$ (I) were treated as indicated followed by lysis and immunoblotting. (J) Annotation enrichment analysis of candidate GABARAPL2-interacting proteins with $\log_2$ SILAC H/L ratios ≥1.5 or ≤-1.5. The bar graphs show significantly overrepresented UniProt keywords.

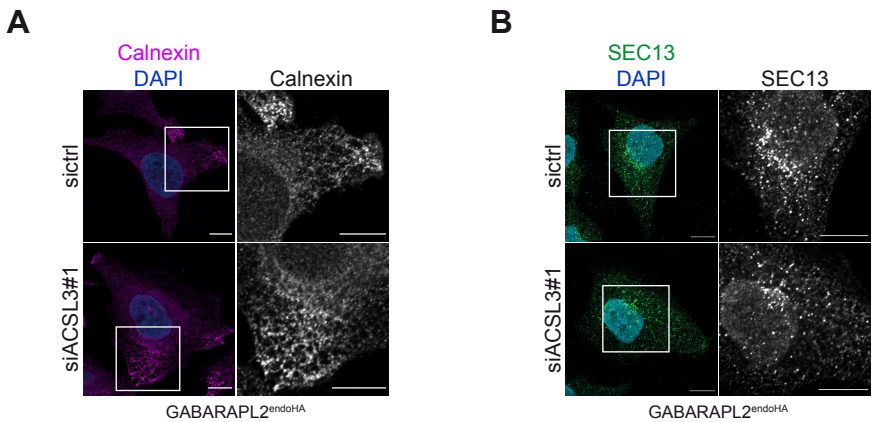

Figure S3

Fig. S3. ACSL3 is not an autophagy substrate. (A,B) GABARAPL2$_{endoHA}$/ACSL3$_{endoNeonGreen}$ cells were transfected with indicated siRNAs prior to immunolabeling with Calnexin (A) or SEC13 (B). Scale bar: 10 µm.

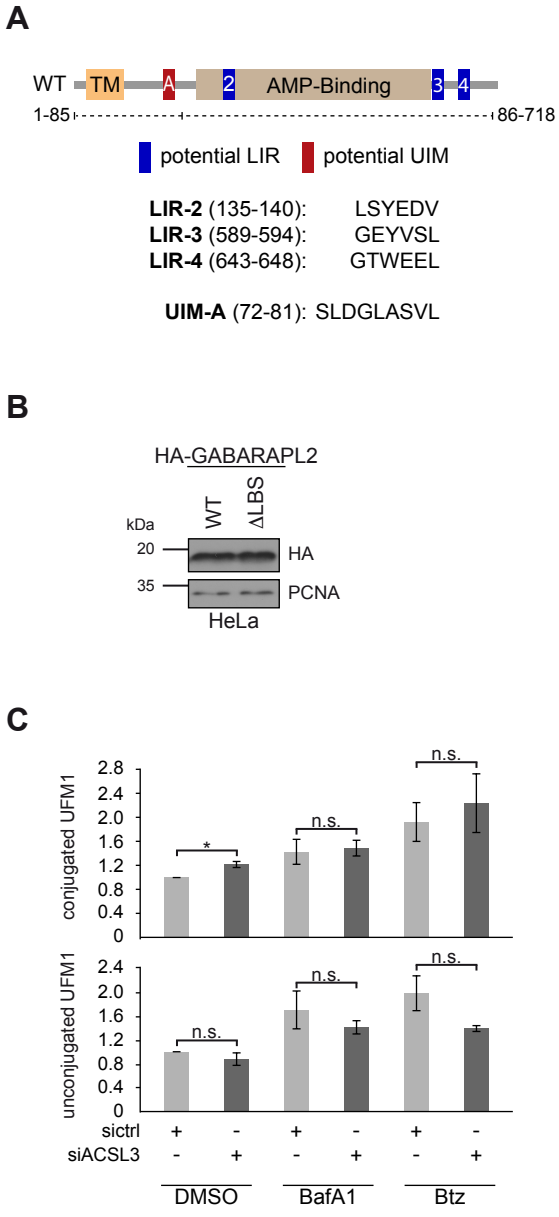
A
WT
TM
A
2
AMP-Binding
3
4
1-85
86-718
potential LIR
potential UIM
LIR-2 (135-140): LSYEDV
LIR-3 (589-594): GEYVSL
LIR-4 (643-648): GTWEEL
UIM-A (72-81): SLDGLASVL
B
HA-GABARAPL2
WT
ΔLBS
kDa
20
35
HA
PCNA
HeLa
C
conjugated UFM1
unconjugated UFM1
n.s.
*
siCtrl
siACSL3
DMSO
BafA1
Btz
D
ACSL3
GABARAPL2
unconjugated UFM1
conjugated UFM1
n.s.
*
0.5
4
8
EtOH (hrs)
oleic acid (hrs)

Figure S4

Fig. S4. Effects of ACSL3 depletion and LD induction on ufmylation. (A) Amino acid sequences of potential LIRs and UIM in ACSL3. (B) Immunoblot analysis of HeLa cells stably expressing wild-type (WT) and LIR-binding deficient (ΔLBS) GABARAPL2. (C) Quantitative analysis from Fig. 7A. Data represents mean ±SEM. Statistical analysis (n = 3) of the indicated protein/PCNA ratio normalized to sictrl-DMSO was performed using Student's t-test (*p<0.05, **p<0.01, ***p<0.001). (D) Quantitative analysis of Fig. 7C. Data represents mean ±SEM. Statistical analysis (n = 3) of the indicated protein/PCNA ratio normalized to 0.5 hrs EtOH was performed using Student's t-test (*p<0.05, **p<0.01).